

Effective properties of hierarchical fiber-reinforced composites via a three-scale asymptotic homogenization approach

*Original*

Effective properties of hierarchical fiber-reinforced composites via a three-scale asymptotic homogenization approach / RAMIREZ TORRES, Ariel; Penta, Raimondo; Rodriguez-Ramos, Reinaldo; Grillo, Alfio. - In: MATHEMATICS AND MECHANICS OF SOLIDS. - ISSN 1081-2865. - 24:11(2019), pp. 3554-3574. [10.1177/1081286519847687]

*Availability:*

This version is available at: 11583/2796550 since: 2020-06-04T21:17:25Z

*Publisher:*

Sage Publications

*Published*

DOI:10.1177/1081286519847687

*Terms of use:*

This article is made available under terms and conditions as specified in the corresponding bibliographic description in the repository

*Publisher copyright*

Sage postprint/Author's Accepted Manuscript

RAMIREZ TORRES, Ariel; Penta, Raimondo; Rodriguez-Ramos, Reinaldo; Grillo, Alfio, Effective properties of hierarchical fiber-reinforced composites via a three-scale asymptotic homogenization approach, accepted for publication in MATHEMATICS AND MECHANICS OF SOLIDS (24 11) pp. 3554-3574. © 2019 (Copyright Holder).  
DOI:10.1177/1081286519847687

(Article begins on next page)

# Effective properties of hierarchical fiber-reinforced composites via a three-scale asymptotic homogenization approach

Ariel Ramírez-Torres<sup>1</sup>, Raimondo Penta<sup>2</sup>, Reinaldo Rodríguez-Ramos<sup>3</sup>, and Alfio Grillo<sup>1</sup>

<sup>1</sup>Dipartimento di Scienze Matematiche “G. L. Lagrange” Politecnico di Torino, 10129.  
Torino, Italia

<sup>2</sup>School of Mathematics and Statistics, Mathematics and Statistics Building, University of  
Glasgow, University Place, Glasgow G128QQ, UK

<sup>3</sup>Departamento de Matemáticas, Facultad de Matemática y Computación, Universidad de  
La Habana, CP 10400, La Habana, Cuba

## Abstract

The study of the properties of multiscale composites is of great interest in engineering and biology. Particularly, hierarchical composite structures can be found in nature and in engineering. During the past decades, the multiscale asymptotic homogenization technique has shown its potential in the description of such composites by taking advantage of their characteristics at the smaller scales, ciphered in the so-called *effective coefficients*. Here, we extend previous works by studying the in-plane and out-of-plane effective properties of hierarchical linear elastic solid composites via a three-scale asymptotic homogenization technique. In particular, the approach is adjusted for a multiscale composite with a square-symmetric arrangement of uniaxially aligned cylindrical fibers, and the formulae for computing its effective properties are provided. Finally, we show the potential of the proposed asymptotic homogenization procedure by modeling the effective properties of musculoskeletal mineralized tissues, and we compare the results with theoretical and experimental data for bone and tendon tissues.

**Keywords** Hierarchical composites, Three-scale asymptotic homogenization, Fiber-reinforced composites, Musculoskeletal mineralized tissues, Effective coefficients

## 1 Introduction

Hierarchical solids are multiscale materials made of different phases which themselves exhibit a finer scale structure. Several examples of the existence of hierarchical composite structures can be found in nature such as musculoskeletal mineralized tissues (MMTs), lotus leaves, among many others. Nowadays, the study of the physical properties of multiscale composite materials is of great interest due to its utility, for instance, in the modeling and design of bioinspired and biomimetic hierarchical materials [5, 28, 64]. In particular, MMTs constitute a widely studied class of hierarchical composite materials. For instance, we refer to the compilation of articles edited by Cowin [13] on structural and mechanical properties of bone.

The different homogenization techniques used in the modeling of multiscale composites have the important advantage of decoupling the structural characteristic lengths. In the case of linear elastic composite materials, the scientific literature develops in two main approaches, the asymptotic homogenization and the average field theory (see, e.g., the review paper [26] and references therein). On one hand, average field

28 techniques [22, 33] aim to find the effective elastic properties which relate the fine scale strain and stress  
29 averages over a representative volume, characterizing, in an ideal form, the heterogeneity of the material.  
30 On the other hand, the asymptotic homogenization technique [6, 7, 10, 55, 3] exploits the scales separation  
31 among the characteristic lengths of the local structures and the one of the whole material by employing  
32 multiple scale expansions of the fields.

33 The multiscale asymptotic homogenization techniques take advantage of the information available at the  
34 smaller scales to obtain an effective description of the medium or phenomenon at its larger scales. In the  
35 scientific literature, there exist several works focusing on modeling and simulation of the macroscopic prop-  
36 erties of hierarchical composite materials using average field techniques [31, 4, 37, 21], reiterated asymptotic  
37 homogenization [7, 30, 2, 14, 58, 29, 53, 16, 61, 35] and hybrid models [41]. For instance, starting from  
38 the basic equations of the phases of a composite featuring a heterogeneous structure over several separated  
39 scales, [30] achieved to deduce the phenomenological equations of a porous medium and, in the process,  
40 the authors also obtained the governing equations for the intermediate scales of the mixture. Afterwards, a  
41 rigorous foundation of the technique was given in [2] who focused on the heat equation for composites and  
42 in [60], a further generalization of the reiterated homogenization technique was introduced via a three-scale  
43 convergence approach providing a groundwork where the asymptotic parameters independently approach  
44 zero. Moreover, in [53], the authors adopted an asymptotic homogenization technique to obtain a homoge-  
45 nized model for a fluid saturated porous medium containing double porous substructures by considering a  
46 hierarchical porous arrangement. In the study conducted by [16], recurrent sequences of local and averaged  
47 elasticity problems for a fiber reinforced composite were written through the introduction of a power series  
48 expansion for each level. Furthermore, in [61], the authors considered a hierarchical laminated composite  
49 with the particularity that the microstructure presented a combination of linear and non-linear generalized  
50 periodicity. Therein, the solution of the problem was sought via a multi-step homogenization approach.  
51 In addition, a step-by-step approach to study the properties of bone using models of micromechanics and  
52 composite laminate theory was followed in [37] and [21]. Finally, the approach proposed by [41] uses a  
53 combination of Eshelby based techniques with the asymptotic homogenization to analyze in a bottom-up  
54 process the stiffening of old bone tissues. From a computational point of view, the work by [65] proposes  
55 a methodology for the development of adaptive methods for hierarchical modeling of elastic heterogeneous  
56 bodies.

57 In this work, we exploit the three-scale asymptotic homogenization approach developed in [47, 48] to  
58 investigate the effective properties of linear elastic, hierarchical, fiber-reinforced composites. The three-  
59 scale homogenization approach permits to individualize each hierarchical level and to investigate how the  
60 properties at the lower scales influence the effective ones in a single scheme. In a previous work [47], the  
61 three-scale asymptotic technique has been applied to compute the effective shear modulus for hierarchical  
62 fiber-reinforced composites. Here, we go further and propose a procedure to compute the effective in-  
63 plane elastic coefficients, which involve the solution of coupled elastic problems. Furthermore, we show  
64 the potential of the multiscale asymptotic homogenization process by applying it to a biological scenario  
65 of interest. Specifically, we are interested in modeling the effective properties of MMTs by performing a  
66 parametric analysis of the mineral crystals' volume fraction. Since the goal is to offer a modeling tool for  
67 studying hierarchical composites, we conveniently adopt the modeling assumptions made in [59]·[41]. In [59],  
68 the authors studied the elastic stiffness tensor of a mineralized turkey leg tendon tissue using a multiscale  
69 model based on average fields Eshelby techniques, such as the Mori-Tanaka and the self-consistent schemes.  
70 In [41], the approach in [59] was extended to the asymptotic homogenization technique by means of a hybrid  
71 hierarchical modeling framework applicable to MMTs, and capable to account for fused mineral structures  
72 in the composite tissue. The results of the present framework are consistent with the experimental and  
73 theoretical data reported in [59, 41].

74 The manuscript is organized as follows. First, the physical and mathematical framework of the problem  
75 is introduced. Next, we present the principal results of the three-scale asymptotic homogenization technique  
76 and address the general local problems associated to each hierarchical level. The in-plane and out-of-plane  
77 local problems for uniaxially fiber-reinforced hierarchical composites with isotropic constituents are also  
78 specified. In addition, the form of the effective coefficients is provided. Furthermore, we compute the

79 effective properties of MMTs and compare the results with experimental and numerical data provided in the  
80 scientific literature. Finally, we discuss the current approach and give directions for future developments of  
81 the study.

## 82 2 Formulation of the problem

### 83 2.1 Geometrical description

84 Let us denote by  $\Omega \subset \mathbb{R}^3$  a multiscale composite characterized by three well-separated characteristics lengths  
85 (see Fig. 1), namely  $\ell_1$ ,  $\ell_2$  and  $L$ , and introduce the scaling parameters  $\varepsilon_1$  and  $\varepsilon_2$  as follows,

$$\varepsilon_1 = \frac{\ell_1}{L} \ll 1 \quad \text{and} \quad \varepsilon_2 = \frac{\ell_2}{L} \ll \varepsilon_1. \quad (1)$$

86 We note that in (1), we have amended a typo on the definition of  $\varepsilon_2$  in previous works [47, 48]. From relation  
87 (1), two formally independent variables are introduced, i.e.

$$\eta = \frac{x}{\varepsilon_1} \quad \text{and} \quad \varsigma = \frac{x}{\varepsilon_2}. \quad (2)$$

88 In what follows, we consider each field and material property  $\Phi^\varepsilon$  to be  $\eta$ - and  $\varsigma$ - periodic and we introduce  
89 the notation  $\Phi^\varepsilon(x) = \Phi(x, \eta, \varsigma)$ .

90 At the first hierarchical level, the composite  $\Omega$  comprises two solid constituents and is partitioned into  
91 two sub-domains  $\Omega_m^{\varepsilon_1}$  and  $\Omega_f^{\varepsilon_1}$ . The former denotes the host (or matrix) phase and the latter represents a  
92 finite collection of disjoints subphases (e.g. inclusions or fibers). Specifically,  $\bar{\Omega} = \bar{\Omega}_m^{\varepsilon_1} \cup \bar{\Omega}_f^{\varepsilon_1}$  with  $\bar{\Omega}_m^{\varepsilon_1} \cap \Omega_f^{\varepsilon_1} =$   
93  $\Omega_m^{\varepsilon_1} \cap \bar{\Omega}_f^{\varepsilon_1} = \emptyset$  and we denote with  $\Gamma^{\varepsilon_1}$  the interface between both constituents  $\Omega_m^{\varepsilon_1}$  and  $\Omega_f^{\varepsilon_1}$ . Furthermore, we  
94 denote by  $\mathcal{Y}$  the unitary periodic cell containing a portion of the host phase  $\mathcal{Y}_m$  and one subphase (or a finite  
95 collection of subphases)  $\mathcal{Y}_f$ . We enforce that the constituents of each periodic cell satisfy that  $\bar{\mathcal{Y}} = \bar{\mathcal{Y}}_m \cup \bar{\mathcal{Y}}_f$   
96 with  $\bar{\mathcal{Y}}_m \cap \mathcal{Y}_f = \mathcal{Y}_m \cap \bar{\mathcal{Y}}_f = \emptyset$ , and we indicate with  $\Gamma_{\mathcal{Y}}$  the interface between  $\mathcal{Y}_m$  and  $\mathcal{Y}_f$ .

97 At the second hierarchical level, we consider that each subphase  ${}_i\Omega_f^{\varepsilon_1}$  ( $i = 1, \dots, N$ ) is also a composite  
98 material with periodic structure. We suppose that each subphase  ${}_i\Omega_f^{\varepsilon_1}$  is composed of a host phase  $\Omega_m^{\varepsilon_2}$  with  
99 a finite number of subphases denoted by  $\Omega_f^{\varepsilon_2}$ . In particular, we assume that for each  $i$ ,  ${}_i\bar{\Omega}_f^{\varepsilon_1} = \bar{\Omega}_m^{\varepsilon_2} \cup \bar{\Omega}_f^{\varepsilon_2}$  with  
100  $\bar{\Omega}_m^{\varepsilon_2} \cap \Omega_f^{\varepsilon_2} = \Omega_m^{\varepsilon_2} \cap \bar{\Omega}_f^{\varepsilon_2} = \emptyset$  and the interface between  $\Omega_m^{\varepsilon_2}$  and  $\Omega_f^{\varepsilon_2}$  is denoted with  $\Gamma^{\varepsilon_2}$ . At this hierarchical  
101 level,  $\mathcal{Z}$  stands for the unitary periodic cell containing a portion of the host phase indicated with  $\mathcal{Z}_m$  and  
102 one subphase (or a finite collection of subphases)  $\mathcal{Z}_f$ . Analogously to the upper hierarchical level, we impose  
103 that  $\bar{\mathcal{Z}} = \bar{\mathcal{Z}}_m \cup \bar{\mathcal{Z}}_f$ , with  $\bar{\mathcal{Z}}_m \cap \mathcal{Z}_f = \mathcal{Z}_m \cap \bar{\mathcal{Z}}_f = \emptyset$  and we indicate with  $\Gamma_{\mathcal{Z}}$  the interface between  $\mathcal{Z}_m$  and  $\mathcal{Z}_f$ .

104 In Table 1, we resume the symbols used in this work.

Table 1: Description of symbols.

Symbol	Description
$\Omega$	Multiscale composite body
$\Omega_m^{\varepsilon_1}$ ( $\Omega_m^{\varepsilon_2}$ )	Host (or matrix) phase at the $\varepsilon_1$ ( $\varepsilon_2$ )-hierarchical level
$\Omega_f^{\varepsilon_1}$ ( $\Omega_f^{\varepsilon_2}$ )	Finite collection of disjoints subphases at the $\varepsilon_1$ ( $\varepsilon_2$ )-hierarchical level
$\Gamma^{\varepsilon_1}$ ( $\Gamma^{\varepsilon_2}$ )	Interface between constituents $\Omega_m^{\varepsilon_1}$ and $\Omega_f^{\varepsilon_1}$ ( $\Omega_m^{\varepsilon_2}$ and $\Omega_f^{\varepsilon_2}$ )
$\mathcal{Y}$ ( $\mathcal{Z}$ )	Unitary periodic cell at the $\varepsilon_1$ ( $\varepsilon_2$ )-hierarchical level
$\mathcal{Y}_m$ ( $\mathcal{Z}_m$ )	Portion of $\Omega_m^{\varepsilon_1}$ ( $\Omega_m^{\varepsilon_2}$ ) contained in the unitary cell $\mathcal{Y}$ ( $\mathcal{Z}$ )
$\mathcal{Y}_f$ ( $\mathcal{Z}_f$ )	Finite collection of subphases $\Omega_f^{\varepsilon_1}$ ( $\Omega_f^{\varepsilon_2}$ ) contained in the unitary cell $\mathcal{Y}$ ( $\mathcal{Z}$ )
$\Gamma_{\mathcal{Y}}$ ( $\Gamma_{\mathcal{Z}}$ )	Interface between $\mathcal{Y}_m$ and $\mathcal{Y}_f$ ( $\mathcal{Z}_m$ and $\mathcal{Z}_f$ )

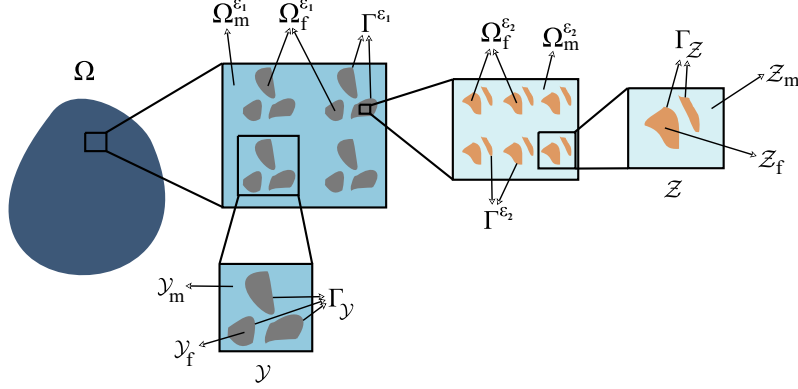


Figure 1: Schematic of the cross-section of a hierarchical periodic composite with three structural levels.

## 2.2 Formulation of the problem

We consider that the constitutive response of all the constituents of the hierarchical composite body  $\Omega$  is linear elastic. This assumption implies that the constituents' constitutive relationships are all given by the formula,

$$\boldsymbol{\sigma}^\varepsilon = \mathcal{C}^\varepsilon : \mathbf{E}(\mathbf{u}^\varepsilon), \quad (3)$$

where  $\mathbf{E}(\mathbf{u}^\varepsilon) := \text{Sym}(\text{Grad}\mathbf{u}^\varepsilon)$  represents the strain tensor under the hypothesis of small displacements  $\mathbf{u}^\varepsilon$ , and  $\mathcal{C}^\varepsilon$  is the fourth-order, positive definite elasticity tensor with both major and minor symmetries, i.e., component-wise,  $\mathcal{C}_{ijkl}^\varepsilon = \mathcal{C}_{jikl}^\varepsilon = \mathcal{C}_{ijlk}^\varepsilon = \mathcal{C}_{klji}^\varepsilon$  ( $i, j, k, l = 1, 2, 3$ ), which is supposed to be phase-wise smooth.

Then, ignoring inertia and volume forces, the differential problem arising from the (local) balance of linear momentum when equipped, for example, with Dirichlet-Neumann external boundary conditions reads

$$(\mathcal{P}^\varepsilon) \begin{cases} \text{Div}[\mathcal{C}^\varepsilon : \mathbf{E}(\mathbf{u}^\varepsilon)] = \mathbf{0}, & \text{in } \Omega \setminus (\Gamma^{\varepsilon_1} \cup \Gamma^{\varepsilon_2}), \\ \mathbf{u}^\varepsilon = \mathbf{u}^*, & \text{on } \partial\Omega_D, \\ [\mathcal{C}^\varepsilon : \mathbf{E}(\mathbf{u}^\varepsilon)] \cdot \mathbf{N} = \mathbf{S}^*, & \text{on } \partial\Omega_N, \end{cases} \quad (4)$$

where  $\mathbf{N}$  is the outward unit vector field normal to the boundary  $\partial\Omega$  of  $\Omega$ ,  $\mathbf{u}^*$  is the displacement field prescribed on the Dirichlet portion of  $\partial\Omega$ , i.e.  $\partial\Omega_D$ , and  $\mathbf{S}^*$  is the field of tractions imposed on the Neumann boundary  $\partial\Omega_N$ . It holds that  $\partial\Omega = \partial\Omega_D \cup \partial\Omega_N$ , with  $\partial\Omega_D \cap \partial\Omega_N = \emptyset$ . Furthermore, continuity conditions for displacements and traction are imposed on both  $\Gamma^{\varepsilon_1}$  and  $\Gamma^{\varepsilon_2}$ , i.e.

$$\llbracket \mathbf{u}^\varepsilon \rrbracket = \mathbf{0}, \quad \text{on } \Gamma^{\varepsilon_1} \cup \Gamma^{\varepsilon_2}, \quad (5a)$$

$$\llbracket (\mathcal{C}^\varepsilon : \mathbf{E}(\mathbf{u}^\varepsilon)) \cdot \mathbf{N}_y \rrbracket = \mathbf{0}, \quad \text{on } \Gamma^{\varepsilon_1}, \quad (5b)$$

$$\llbracket (\mathcal{C}^\varepsilon : \mathbf{E}(\mathbf{u}^\varepsilon)) \cdot \mathbf{N}_z \rrbracket = \mathbf{0}, \quad \text{on } \Gamma^{\varepsilon_2}, \quad (5c)$$

where  $\mathbf{N}_y$  and  $\mathbf{N}_z$  represent the outward unit vectors normal to the surfaces  $\Gamma^{\varepsilon_1}$  and  $\Gamma^{\varepsilon_2}$ , respectively. The operator  $\llbracket \Phi^\varepsilon \rrbracket$  denotes the jump of  $\Phi^\varepsilon$  across the interface between two constituents in the same hierarchical level.

## 3 Three-scale asymptotic homogenization procedure

The property of separation of scales together with definition (2), imply that,

$$\text{Grad}\Phi^\varepsilon(x) = \text{Grad}_x\Phi(x, \eta, \varsigma) + \varepsilon_1^{-1}\text{Grad}_\eta\Phi(x, \eta, \varsigma) + \varepsilon_2^{-1}\text{Grad}_\varsigma\Phi(x, \eta, \varsigma), \quad (6)$$

123 where the chain rule has been used, and the sub-indices of the gradient operators on the right-hand-side  
 124 indicate that the derivative is performed with respect to  $x$ ,  $\eta$ , and  $\varsigma$ . In addition, the following average  
 125 operators over the periodic cells  $\mathcal{Y}$  and  $\mathcal{Z}$  are introduced,

$$\langle \Phi^\varepsilon(x) \rangle_\eta = \frac{1}{|\mathcal{Y}|} \int_{\mathcal{Y}} \Phi(x, \eta, \varsigma) d\eta, \quad (7a)$$

$$\langle \Phi^\varepsilon(x) \rangle_\varsigma = \frac{1}{|\mathcal{Z}|} \int_{\mathcal{Z}} \Phi(x, \eta, \varsigma) d\varsigma, \quad (7b)$$

126 where  $|\mathcal{Y}|$  and  $|\mathcal{Z}|$  denote the volume fractions of the periodic cells  $\mathcal{Y}$  and  $\mathcal{Z}$ , respectively.

127 At this stage, we perform a three-scale asymptotic expansion for the displacement  $\mathbf{u}^\varepsilon$  in powers of the  
 128 scaling parameters  $\varepsilon_1$  and  $\varepsilon_2$ . Specifically, we impose that

$$\mathbf{u}^\varepsilon(x) = \tilde{\mathbf{u}}^{(0)}(x, \eta, \varsigma) + \sum_{i=1}^{+\infty} \tilde{\mathbf{u}}^{(i)}(x, \eta, \varsigma) \varepsilon_2^i, \quad (8)$$

129 where

$$\tilde{\mathbf{u}}^{(0)}(x, \eta, \varsigma) = \mathbf{u}^{(0)}(x, \eta, \varsigma) + \sum_{j=1}^{+\infty} \mathbf{u}^{(j)}(x, \eta, \varsigma) \varepsilon_1^j. \quad (9)$$

130 Now, we embrace the homogenization process illustrated in [47, 48]. That is, we first substitute the expansion  
 131 (8) into the original problem constituted by equations (4) and (5a)-(5c), and then, we equate the resulting  
 132 expressions in powers of  $\varepsilon_2$ , and subsequently, using (9), in powers of  $\varepsilon_1$ .

133 Following this procedure, it can be shown that the term  $\mathbf{u}^{(0)}$  is a function of the “slow” variable only,  
 134 i.e.,  $\mathbf{u}^{(0)}(x, \eta, \varsigma) \equiv \mathbf{u}^{(0)}(x)$ , and solution of the *homogenized problem*

$$(\mathcal{P}) \begin{cases} \text{Div}_x[\hat{\mathcal{C}} : \mathbf{E}_x(\mathbf{u}^{(0)})] = \mathbf{0}, & \text{in } \Omega_h, \\ \mathbf{u}^{(0)} = \mathbf{u}^*, & \text{on } \partial\Omega_D^h, \\ [\hat{\mathcal{C}} : \mathbf{E}_x(\mathbf{u}^{(0)})] \cdot \mathbf{N} = \mathbf{S}^*, & \text{on } \partial\Omega_N^h, \end{cases} \quad (10)$$

135 where  $\Omega_h$  represents the homogeneous macro-scale domain in which the homogenized equations are defined.  
 136 In (10),  $\hat{\mathcal{C}}$  represents the *effective fourth-order elasticity tensor* of the hierarchical composite material, which  
 137 is given by the formula

$$\hat{\mathcal{C}} = \langle \mathcal{C}^{\varepsilon_1} + \mathcal{C}^{\varepsilon_1} : \mathbf{T}\mathbf{E}_\eta(\boldsymbol{\omega}) \rangle_\eta, \quad (11)$$

138 where the fourth-order tensor  $\mathcal{C}^{\varepsilon_1}$  is given by

$$\mathcal{C}^{\varepsilon_1}(x) = \begin{cases} \mathcal{C}^{m,\eta}(x, \eta), & \eta \in \Omega_m^{\varepsilon_1}, \\ \mathcal{C}^{f,\eta}(x, \eta), & \eta \in \Omega_f^{\varepsilon_1}. \end{cases} \quad (12)$$

139 In (12),  $\mathcal{C}^{m,\eta}$  and  $\mathcal{C}^{f,\eta}$  represent the elasticity tensors corresponding to the constituents  $\Omega_m^{\varepsilon_1}$  and  $\Omega_f^{\varepsilon_1}$ ,  
 140 respectively. Furthermore,  $\boldsymbol{\omega}$  is a third-order,  $\eta$ -periodic tensor field such that

$$\mathbf{u}^{(1)}(x, \eta, \varsigma) \equiv \mathbf{u}^{(1)}(x, \eta) = \boldsymbol{\omega}(x, \eta) : \mathbf{E}_x[\mathbf{u}^{(0)}(x)], \quad (13)$$

141 with  $\mathbf{E}_x[\mathbf{u}^{(0)}(x)] := \text{Sym}[\text{Grad}_x \mathbf{u}^{(0)}(x)]$ . Moreover,  $\mathbf{T}\mathbf{E}_\beta(\boldsymbol{\omega}) = \frac{1}{2}[\text{TGrad}_\beta \boldsymbol{\omega} + {}^t(\text{TGrad}_\beta \boldsymbol{\omega})]$ , with  $\beta = x, \eta, \varsigma$   
 142 (see [49]). The operation  ${}^t(\mathcal{A})$  transposes the fourth-order tensor  $\mathcal{A}$  by exchanging the order of its first pair  
 143 of indices only, and  $\text{TGrad}_\beta \boldsymbol{\omega}$  is the fourth-order tensor defined as

$$\text{TGrad}_\beta \boldsymbol{\omega} = \frac{\partial \omega_{ijkl}}{\partial \beta_j} \mathbf{e}_i \otimes \mathbf{e}_j \otimes \mathbf{e}_k \otimes \mathbf{e}_l. \quad (14)$$

144 Note that we are not using the covariant formalism in this work, otherwise the partial differentiation on the  
 145 right-hand-side of (14) should be substituted with a covariant derivative.

146 Particularly, the third-order tensor field  $\boldsymbol{\omega}$  is determined by solving the following auxiliary cell problem

$$(\mathcal{P}_Y) \begin{cases} \text{Div}_\eta[\mathcal{C}^{\varepsilon_1} + \mathcal{C}^{\varepsilon_1} : \mathbf{T}\mathbf{E}_\eta(\boldsymbol{\omega})] = \mathbf{0}, & \text{in } Y \setminus \Gamma_Y, \\ [(\mathcal{C}^{\varepsilon_1} + \mathcal{C}^{\varepsilon_1} : \mathbf{T}\mathbf{E}_\eta(\boldsymbol{\omega})) \cdot \mathbf{N}_Y] = \mathbf{0}, & \text{on } \Gamma_Y, \\ [\boldsymbol{\omega}] = \mathbf{0}, & \text{on } \Gamma_Y, \end{cases} \quad (15)$$

147 where the condition  $\langle \boldsymbol{\omega} \rangle_\eta = \mathbf{0}$  is imposed to guarantee uniqueness in the local problem (15). We remark that  
 148 the condition of zero average of the third-order tensor  $\boldsymbol{\omega}$  is just one particular way, without losing generality,  
 149 to close the problem (15).

150 At this point we note that in this formulation (see [47, 48] for more details), the homogenization process  
 151 accomplishes to relate the length scales in a cascade mode from the lower to the higher one, so that, the  
 152 fourth-order elasticity tensor  $\mathcal{C}^{\mathbf{f},\eta}$  in (12), corresponding to the constituent  $\Omega_f^{\varepsilon_1}$ , is in fact, an effective one,  
 153 and is given through the formula

$$\mathcal{C}^{\mathbf{f},\eta} \equiv \check{\mathcal{C}} = \langle \mathcal{C}^{\varepsilon_2} + \mathcal{C}^{\varepsilon_2} : \mathbf{T}\mathbf{E}_\varsigma(\tilde{\boldsymbol{\omega}}) \rangle_\varsigma. \quad (16)$$

154 We denote with  $\check{\mathcal{C}}$  the *effective fourth-order elasticity tensor at the  $\varepsilon_1$ -hierarchical level* of the composite  
 155 material. In particular, for  $\eta \in \Omega_f^{\varepsilon_1}$ ,

$$\mathcal{C}^{\varepsilon_2}(x) = \begin{cases} \mathcal{C}^{\mathbf{m},\varsigma}(x, \eta, \varsigma), & \varsigma \in \Omega_m^{\varepsilon_2}, \\ \mathcal{C}^{\mathbf{f},\varsigma}(x, \eta, \varsigma), & \varsigma \in \Omega_f^{\varepsilon_2}, \end{cases} \quad (17)$$

156 where  $\mathcal{C}^{\mathbf{m},\varsigma}$  and  $\mathcal{C}^{\mathbf{f},\varsigma}$  denote the elasticity tensors corresponding to the constituents  $\Omega_m^{\varepsilon_2}$  and  $\Omega_f^{\varepsilon_2}$ , respectively.  
 157 In (16),  $\tilde{\boldsymbol{\omega}}$  is a third-order,  $\varsigma$ - and  $\eta$ -periodic tensor field such that

$$\begin{aligned} \tilde{\boldsymbol{u}}^{(1)}(x, \eta, \varsigma) &= \tilde{\boldsymbol{\omega}}(x, \eta, \varsigma) : (\mathcal{I} + \mathbf{T}\mathbf{E}_\eta[\boldsymbol{\omega}(x, \eta)]) : \mathbf{E}_x[\mathbf{u}^{(0)}(x)] \\ &\quad + \tilde{\boldsymbol{\omega}}(x, \eta, \varsigma) : \mathbf{T}\mathbf{E}_x[\boldsymbol{\omega}(x, \eta)] : \mathbf{E}_x[\mathbf{u}^{(0)}(x)]_{\varepsilon_1}, \end{aligned} \quad (18)$$

158 where  $\mathcal{I}$  is the fourth-order identity tensor, i.e., for every symmetric tensor  $\mathbf{A}$ , it holds that  $\mathcal{I} : \mathbf{A} = \mathbf{A}$ .  
 159 Furthermore, the tensor  $\tilde{\boldsymbol{\omega}}$  is solution of the cell problem

$$(\mathcal{P}_Z) \begin{cases} \text{Div}_\varsigma[\mathcal{C}^{\varepsilon_2} + \mathcal{C}^{\varepsilon_2} : \mathbf{T}\mathbf{E}_\varsigma(\tilde{\boldsymbol{\omega}})] = \mathbf{0}, & \text{in } Z \setminus \Gamma_Z, \\ [(\mathcal{C}^{\varepsilon_2} + \mathcal{C}^{\varepsilon_2} : \mathbf{T}\mathbf{E}_\varsigma(\tilde{\boldsymbol{\omega}})) \cdot \mathbf{N}_Z] = \mathbf{0}, & \text{on } \Gamma_Z, \\ [\tilde{\boldsymbol{\omega}}] = \mathbf{0}, & \text{on } \Gamma_Z, \end{cases} \quad (19)$$

160 where the condition  $\langle \tilde{\boldsymbol{\omega}} \rangle_\varsigma = \mathbf{0}$  is imposed to guarantee uniqueness in the local problem (19).

## 161 4 Effective properties of hierarchical fiber-reinforced composites

162 In this section, we particularize the results given in the previous section by focusing on a three-scale composite  
 163 material with a square-symmetric arrangement of uniaxially aligned cylindrical fibers (see Fig. 2). For this  
 164 particular case, the three-dimensional cell problems (15) and (19) can be re-formulated as two-dimensional  
 165 local problems defined over the cells' cross-sections corresponding to a square embedding a single circle.

166 Specifically, we assume that at the  $\varepsilon_2$ -hierarchical level, both  $\mathcal{C}^{\mathbf{m},\varsigma}$  and  $\mathcal{C}^{\mathbf{f},\varsigma}$  are piece-wise constant. This  
 167 consideration indicates that the dependence of the cell problem  $\mathcal{P}_Z$  on  $\eta$  and  $x$  is lost, and consequently,  
 168 that the auxiliary third-order tensor  $\tilde{\boldsymbol{\omega}}$  depends only on  $\varsigma$ . Therefore, the effective elasticity tensor at the  
 169  $\varepsilon_1$ -hierarchical level,  $\check{\mathcal{C}}$ , is likewise piece-wise constant. Additionally, considering that  $\mathcal{C}^{\mathbf{m},\eta}$  is piece-wise  
 170 constant, it can be deduced, in a similar way, that  $\boldsymbol{\omega}$  will only depend on  $\eta$  and that the effective elasticity  
 171 tensor,  $\hat{\mathcal{C}}$ , will be piece-wise constant.

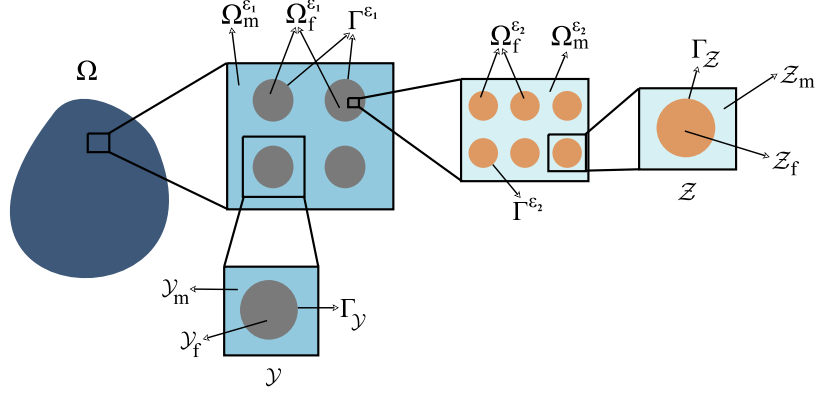


Figure 2: Schematic of the cross-section of a hierarchical fiber-reinforced periodic composite with three structural levels.

172 In like manner, we suppose that all the constituents in  $\Omega$  are isotropic. This assumption together with the  
 173 specified geometrical microstructure at the  $\varepsilon_2$ -hierarchical level implies that  $\mathcal{C}$  is tetragonal symmetric. This  
 174 means that the effective elasticity tensor  $\mathcal{C}$  has six independent elastic coefficients. Moreover, the assumption  
 175 of isotropy of the constituent  $\Omega_m^{\varepsilon_1}$  induces that the effective coefficient  $\mathcal{C}$  is at most monoclinic. Therefore,  
 176 the cell problems  $\mathcal{P}_Z$  and  $\mathcal{P}_Y$  uncouple in sets of equations for the in-plane and out-of-plane stresses. That  
 177 is, the local problems (15) and (19) rewrite, each one, as four in-plane problems  $\mathcal{P}_\alpha^{qq}$  ( $q = 1, 2, 3$ ) and  $\mathcal{P}_\alpha^{12}$ ,  
 178 with  $\alpha = \eta, \varsigma$

$$(\mathcal{P}_\alpha^{qq}) \begin{cases} \frac{\partial \sigma_{11}^{qq\gamma, \alpha}}{\partial \alpha_1} + \frac{\partial \sigma_{12}^{qq\gamma, \alpha}}{\partial \alpha_2} = 0, & \text{in } \tilde{K}_\alpha^\gamma, \\ \frac{\partial \sigma_{21}^{qq\gamma, \alpha}}{\partial \alpha_1} + \frac{\partial \sigma_{22}^{qq\gamma, \alpha}}{\partial \alpha_2} = 0, & \text{in } \tilde{K}_\alpha^\gamma, \\ [[\omega_{1qq}^\alpha]] = 0, \quad [[\omega_{2qq}^\alpha]] = 0, & \text{on } \tilde{\Gamma}_\alpha, \\ [[\sigma_{11}^{qq, \alpha} N_1^\alpha + \sigma_{12}^{qq, \alpha} N_2^\alpha]] = -[[\mathcal{C}_{11qq}^\alpha N_1^\alpha]], & \text{on } \tilde{\Gamma}_\alpha, \\ [[\sigma_{21}^{qq, \alpha} N_1^\alpha + \sigma_{22}^{qq, \alpha} N_2^\alpha]] = -[[\mathcal{C}_{22qq}^\alpha N_2^\alpha]], & \text{on } \tilde{\Gamma}_\alpha, \end{cases} \quad (20a)$$

$$(\mathcal{P}_\alpha^{12}) \begin{cases} \frac{\partial \sigma_{11}^{12\gamma, \alpha}}{\partial \alpha_1} + \frac{\partial \sigma_{12}^{12\gamma, \alpha}}{\partial \alpha_2} = 0, & \text{in } \tilde{K}_\alpha^\gamma, \\ \frac{\partial \sigma_{21}^{12\gamma, \alpha}}{\partial \alpha_1} + \frac{\partial \sigma_{22}^{12\gamma, \alpha}}{\partial \alpha_2} = 0, & \text{in } \tilde{K}_\alpha^\gamma, \\ [[\omega_{1qq}^\alpha]] = 0, \quad [[\omega_{2qq}^\alpha]] = 0, & \text{on } \tilde{\Gamma}_\alpha, \\ [[\sigma_{11}^{12\alpha} N_1^\alpha + \sigma_{12}^{12\alpha} N_2^\alpha]] = -[[\mathcal{C}_{1212}^\alpha N_2^\alpha]], & \text{on } \tilde{\Gamma}_\alpha, \\ [[\sigma_{21}^{12\alpha} N_1^\alpha + \sigma_{22}^{12\alpha} N_2^\alpha]] = -[[\mathcal{C}_{1212}^\alpha N_1^\alpha]], & \text{on } \tilde{\Gamma}_\alpha, \end{cases} \quad (20b)$$

179 and two anti-plane problems  $\mathcal{P}_\alpha^{3q}$  ( $q = 1, 2$ )

$$(\mathcal{P}_\alpha^{3q}) \begin{cases} \frac{\partial \sigma_{31}^{3q\gamma, \alpha}}{\partial \alpha_1} + \frac{\partial \sigma_{32}^{3q\gamma, \alpha}}{\partial \alpha_2} = 0, & \text{in } \tilde{K}_\alpha^\gamma, \\ [[\omega_{33q}^\alpha]] = 0, & \text{on } \tilde{\Gamma}_\alpha, \\ [[\sigma_{31}^{3q, \alpha} N_1^\alpha + \sigma_{32}^{3q, \alpha} N_2^\alpha]] = -[[\mathcal{C}_{3131}^\alpha N_q^\alpha]], & \text{on } \tilde{\Gamma}_\alpha, \end{cases} \quad (21)$$



180 where  $\gamma = m, f$ , and  $\tilde{K}_\zeta^\gamma := \tilde{Z}_\gamma$  and  $\tilde{K}_\eta^\gamma := \tilde{Y}_\gamma$  denote, respectively, the two-dimensional cross-sections of  $\mathcal{Z}_\gamma$   
 181 and  $\mathcal{Y}_\gamma$ . The interface between the constituents  $\tilde{Z}_m$  and  $\tilde{Z}_f$  ( $\tilde{Y}_m$  and  $\tilde{Y}_f$ ) is denoted by  $\tilde{\Gamma}_Z$  ( $\tilde{\Gamma}_Y$ ).  
 182 Additionally, in (20a)–(21)

$$\omega_{kpq}^\alpha := \begin{cases} \tilde{\omega}_{kpq}, & \text{for } \alpha = \varsigma, \\ \omega_{kpq}, & \text{for } \alpha = \eta, \end{cases} \quad (22)$$

183 and

$$\sigma_{ij}^{pq\gamma, \alpha} := \begin{cases} \mathcal{C}_{ijkl}^{\gamma, \varsigma} \frac{\partial \tilde{\omega}_{kpq}}{\partial \varsigma_l}, & \text{for } \alpha = \varsigma, \\ \mathcal{C}_{ijkl}^{\gamma, \eta} \frac{\partial \omega_{kpq}}{\partial \eta_l}, & \text{for } \alpha = \eta. \end{cases} \quad (23)$$

184 In (23),  $\mathcal{C}_{ijkl}^{\gamma, \varsigma}$  and  $\mathcal{C}_{ijkl}^{\gamma, \eta}$  are the components of the elasticity tensor of the constituent  $\gamma = m, f$  at the  $\varepsilon_2$ - and  
 185  $\varepsilon_1$ -hierarchical levels, respectively.

186 Furthermore, component-wise, the fourth-order effective elasticity tensor at the  $\varepsilon_1$ -hierarchical level  $\hat{\mathcal{C}}$ ,  
 187 and the fourth-order effective elasticity tensor of the hierarchical composite material  $\hat{\mathcal{C}}$ , are

$$\hat{\mathcal{C}}_{ijpq} = \langle \mathcal{C}_{ijpq}^{\varepsilon_2} + \mathcal{C}_{ijkl}^{\varepsilon_2} \frac{\partial \tilde{\omega}_{kpq}}{\partial \varsigma_l} \rangle_\varsigma, \quad (24a)$$

$$\hat{\mathcal{C}}_{ijpq} = \langle \mathcal{C}_{ijpq}^{\varepsilon_1} + \mathcal{C}_{ijkl}^{\varepsilon_1} \frac{\partial \omega_{kpq}}{\partial \eta_l} \rangle_\eta, \quad (24b)$$

188 respectively.

189 The theory of analytical functions in [34] applied to the cell problems (20a)–(21) allow us to find the  
 190 effective coefficients  $\hat{\mathcal{C}}_{ijpq}$  and  $\hat{\mathcal{C}}_{ijpq}$  given in (24a) and (24b), respectively. In the present study we follow  
 191 the procedure adopted in [45, 52, 54, 8] and we adapt it to the obtained scale-coupled cell problems (see  
 192 Appendix). We note that in the previous work [47] we dealt with the solution of the coupled-anti-plane  
 193 cell problems, and therefore only the procedure for the coupled-in-plane cell problems is shown here. In  
 194 particular, the choice of the microstructure and material symmetry, and the generality of the analytical  
 195 approach permit us to focus on the solution of the cell problems in only one hierarchical level. We note that  
 196 due to the algebraic complexity of the analytical formulae for the effective coefficients given by relations  
 197 (53a)–(53d) and (55), we use Matlab in order to solve the infinite linear systems (49) and (51), truncated  
 198 to a fixed order, and, subsequently, to evaluate the results in the corresponding formulae for the effective  
 199 coefficients.

## 200 5 Modeling MMTs' effective properties

201 In the present section we show the potential of the three-scale asymptotic homogenization approach by mod-  
 202 eling the effective properties of MMTs. Bones and tendons are examples of MMTs, which are hierarchically  
 203 structured materials, and whose principal constituents, organized spanning several length scales, are mineral  
 204 crystals, collagen, and water. The principal elements of MMTs are cylindrical mineralized collagen fibrils  
 205 consisting in self-assembled collagen molecules that are aligned in staggered arrays [59]. The hydroxyapatite  
 206 crystals are distributed in both the intrafibrillar space, reinforcing the collagen fibrils, and in the extrafibrillar  
 207 space, which primarily consists of mineral and water (see [59, 62] and references therein).

### 208 5.1 Geometrical model for MMTs

209 In the present work, we consider an approximated model for MMTs. Specifically, at the  $\varepsilon_2$ -hierarchical  
 210 level we suppose that  $\mathcal{Z}_m$  represents the minerals surrounding a single collagen fiber denoted by  $\mathcal{Z}_f$ . The  
 211 collection of all collagen fibers at the  $\varepsilon_2$ -hierarchical level  $\Omega_1^{\varepsilon_2}$ , together with the host phase  $\Omega_m^{\varepsilon_2}$  (representing

212 the minerals) will constitute the mineralized collagen fiber  $\mathcal{Y}_f$  at the  $\varepsilon_1$ -hierarchical level. The finite collection  
 213 of mineralized collagen fibers  $\Omega_f^{\varepsilon_1}$  are supposed to be periodically distributed in the extrafibrillar space  $\Omega_m^{\varepsilon_1}$ .  
 214 The union of the disjoint sets  $\Omega_f^{\varepsilon_1}$  with  $\Omega_m^{\varepsilon_1}$  will form each one of the mineralized collagen fibril bundles.  
 215 Finally, the extrafibrillar space is supposed to be a mixture of water and minerals (see Fig. 3). The situation  
 216 just described, where mineralized collagen fibers are unidirectionally aligned, can be, for example, the case  
 217 of a mineralized turkey leg tendon, and it can be considered as a simplified model for bones [59].

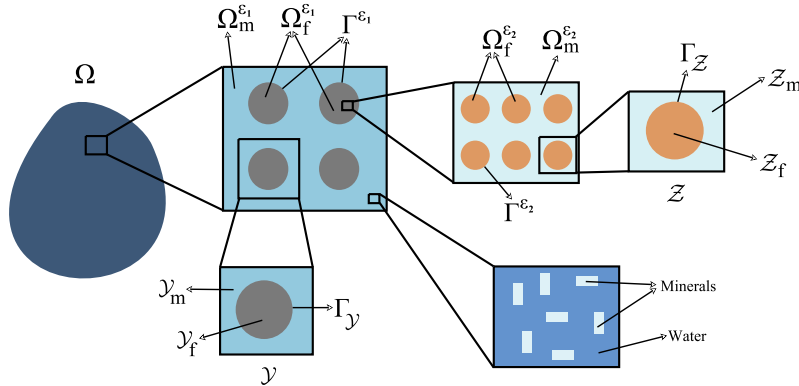


Figure 3: Schematic of the cross-section of MMTs.

218 In order to find the effective properties of the extrafibrillar space we take advantage of Reuss' lower  
 219 bound formula [51] to compute the effective properties of the mixture  $\Omega_m^{\varepsilon_1}$  as follows

$$\mathcal{C}^{m,\eta} = \langle (\mathcal{C}_{ES})^{-1} \rangle^{-1}, \quad (25)$$

220 where

$$\mathcal{C}_{ES}(x) = \begin{cases} \mathcal{C}^{w,\varsigma}(x, \eta, \varsigma), & \text{if } \varsigma \text{ is in the water phase,} \\ \mathcal{C}^{m,\varsigma}(x, \eta, \varsigma), & \text{if } \varsigma \text{ is in the mineral phase.} \end{cases} \quad (26)$$

221 In (26),  $\mathcal{C}^{w,\varsigma}$  and  $\mathcal{C}^{m,\varsigma}$  are the elasticity tensors related to the water and mineral phases, respectively. In  
 222 particular, and following [59], we replace the material properties of water by those of polymethylmethacrylate  
 223 (PMMA).

224 We remark that the present three-scale asymptotic approach can be improved to compute the effective  
 225 properties of the composite extrafibrillar space. However, a realistic geometrical description of the structure  
 226 of the extrafibrillar space requires numerical simulations in three dimensions for elastic composites (see e.g.  
 227 [42, 41, 43]) which are beyond the scope of this work. Here we estimate the effective elastic constants of  
 228 the extrafibrillar space by means of the Reuss bounds, thus obtaining a fully semi-analytic computational  
 229 framework at each hierarchical level of organization. Reuss's formula (25) permits to obtain a lower bound  
 230 for the current model. When we say that we obtain a lower bound for the model, it means that indeed, by  
 231 considering the asymptotic homogenization approach instead, effective values above those computed using  
 232 Reuss' scheme are expected [43].

## 233 5.2 Effective properties of MMTs

234 To model the effective properties of MMTs, we conveniently take advantage of some of the modeling as-  
 235 sumptions in [59], [41]. Specifically, we consider all constituents of the hierarchical composite material are  
 236 isotropic and that correspond to those of a bone tissue [59]. That is, Young's modulus ( $E$ ) and Poisson's  
 237 ratio ( $\nu$ ) of the mineral crystals, collagen fibers and water constituents (individuated by the subscripts m, c  
 238 and p, respectively) are given as reported in Table 2.

Table 2: Young’s modulus and Poisson’s ratio of the mineral crystals, collagen fibers and water constituents.

Parameter	Unit	Value
$E_M$	[GPa]	110
$E_c$	[GPa]	5.00
$E_p$	[GPa]	4.96
$\nu_M$	[-]	0.28
$\nu_c$	[-]	0.30
$\nu_p$	[-]	0.37

Moreover, we perform a parametric analysis of the MMTs’ effective properties by increasing the volume fraction of the mineral crystals, denoted by  $V$ , in the mineralized collagen fibril bundle from 0.2 to 0.5 [59]. Following [59], we also take into account the mineral distribution parameter  $\phi$ , defined as the ratio of the mineral volume in the mineralized collagen fibril to the total mineral volume in the mineralized collagen fibril bundle. In [1], the mineral distribution parameter was estimated to be less than or equal to 0.7, here we chose  $\phi = 0.5$ . Specifically, the parameter  $\phi$  is related to the phase volume fractions using the following empirical formula [50, 59]

$$V^{f,\eta} = \phi V + h(V), \quad (27)$$

where  $h(V) := \frac{\varpi}{1+\varpi}(1 - V)$  and  $\varpi := 0.36 + 0.084 e^{6.7V}$ . In (27), the symbol  $V^{f,\eta}$  represents the volume fraction of the mineralized collagen fibrils in the mineralized collagen fibril bundle. Therefore, the volume fraction of the extrafibrillar space in the mineralized collagen fibril bundle is given by  $V^{m,\eta} = 1 - V^{f,\eta}$ . Additionally, the volume fractions of the mineral crystals ( $V^{m,s}$ ) and of collagen ( $V^{f,s}$ ) in the mineralized collagen fibril are given by [59]

$$V^{m,s} = \phi \frac{V}{V^{f,\eta}} \quad \text{and} \quad V^{f,s} = 1 - V^{m,s}. \quad (28)$$

Finally, the volume fractions of the mineral crystals and water phases in the extrafibrillar space are

$$V^{f,ES} = (1 - \phi) \frac{V}{1 - V^{f,\eta}} \quad \text{and} \quad V^{m,ES} = 1 - V^{f,ES}, \quad (29)$$

respectively.

Figure 4 shows the effective coefficients  $\hat{\mathcal{C}}_{11}$  (left panel) and  $\hat{\mathcal{C}}_{33}$  (right panel), obtained by applying the three-scale homogenization approach, plotted with respect to the degree of mineralization of the tissue. In Fig. 4, we also show a comparison with the theoretical results obtained in [59]. Qualitatively, the results are in agreement with the ones obtained by [59], that is, the effective axial and transverse stiffness coefficients increase with respect to the minerals volume fraction. It is known that the results obtained by the asymptotic homogenization method are closer to those obtained by Reuss formula. Therefore, even in this case, we are positive that using an asymptotic approach for the characterization of the composite extrafibrillar space, the effective elastic coefficients will remain close to those in [59].

It is also known that the asymptotic homogenization technique gives effective properties lying between those computed using Reuss and Voigt formulae (see e.g. [43]). In Fig. 4 (right panel), the results are below those obtained by [59] for  $\hat{\mathcal{C}}_{33}$ . However, for  $\hat{\mathcal{C}}_{11}$ , the results lie above those in [59]. Even though we were not quite expecting this, the curve found with the present approach remains closer to that predicted by [59]. Furthermore, we obtain a satisfactory agreement with experimental data, and actually the obtained bounds are tighter than those in [59], as shown by Fig 5. In Fig. 5, we compare the effective axial and transverse stiffness coefficients with the experimental data showed in [59] corresponding to mineralized turkey leg tendon, human femur and mice bone. As commented before, the results fit very well the experimental

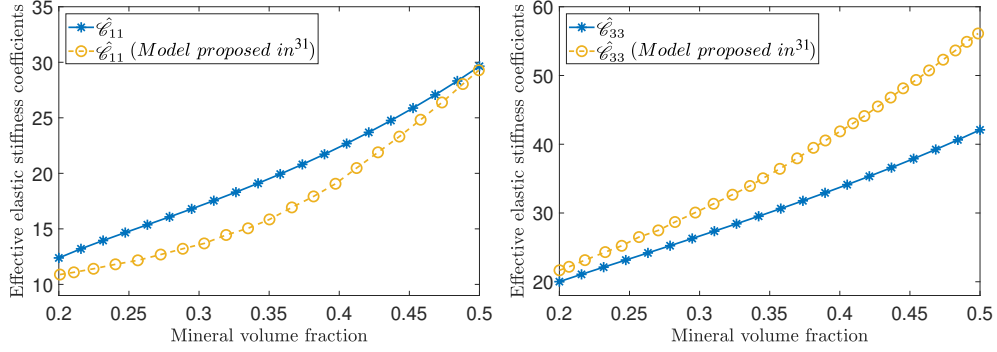


Figure 4: Elastic stiffness coefficients  $\hat{\mathcal{C}}_{11}$  (left) and  $\hat{\mathcal{C}}_{33}$  (right) with respect to the mineral volume fraction  $V$ . A comparison with the theoretical results in [59] are also shown.

269 data. We note that a Voigt formulation for computing the extrafibrillar space’s effective properties is also  
 270 plausible. Indeed, we also considered Voigt upper bounds to model the properties of the extrafibrillar space.  
 271 However, we preferred not to show them since the results did not match well the experimental and theoretical  
 272 data.

273 The results shown in Fig. 5 could be of special interest for clinical applications including, for instance,  
 274 tissue reconstruction. Indeed, following the methodology presented in this work, and considering other  
 275 internal structures and properties, we could assess, in principle, how well fabricated a composite is by  
 276 matching our analytical/computational results with the real properties of a target tissue (see e.g. [23]).  
 277 Since the present homogenization approach takes into consideration three spatial scales, with respect to  
 278 two-scale methods, it provides a better “microscope” to resolve the internal structure of a composite and to  
 279 capture its material properties.

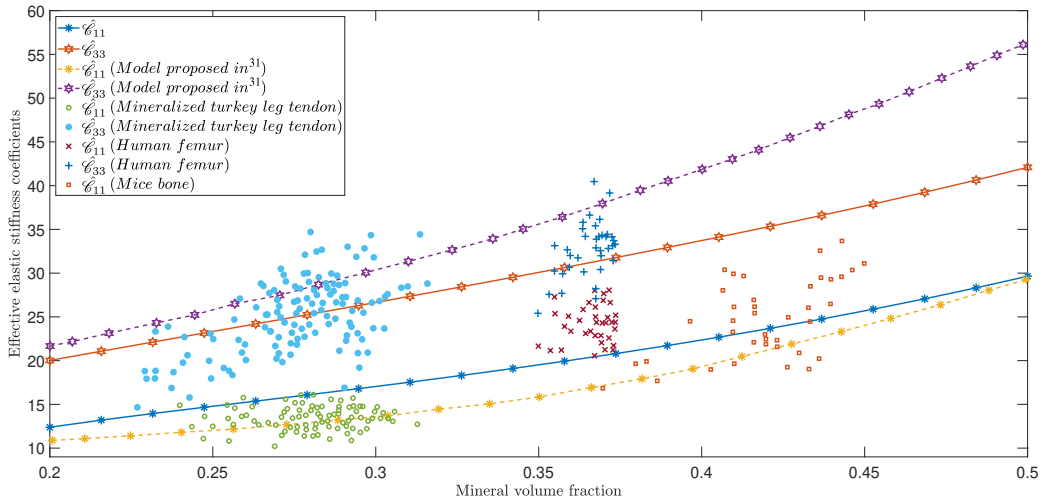


Figure 5: Comparison of the predicted and measured elastic stiffness coefficients  $\hat{\mathcal{C}}_{11}$  (transverse) and  $\hat{\mathcal{C}}_{33}$  (axial) with the experimental and theoretical data reported in [59] (and references therein) corresponding to mineralized turkey tendon leg, human femur and mice bone.

280 For completeness in the analysis we show in Fig. 6 the shear effective elastic coefficients  $\hat{\mathcal{C}}_{44}$ ,  $\hat{\mathcal{C}}_{55}$  and  
 281  $\hat{\mathcal{C}}_{66}$  with respect to the mineral volume fraction. As shown in Fig. 6, the shear coefficients  $\hat{\mathcal{C}}_{44}$ ,  $\hat{\mathcal{C}}_{55}$  and

282  $\hat{\mathcal{C}}_{66}$  increase with increasing tissue's mineralization. Furthermore, the coefficients  $\hat{\mathcal{C}}_{44}$  and  $\hat{\mathcal{C}}_{55}$  coincide. We  
 283 remark that the homogenized elasticity tensor has tetragonal symmetry (6 independent elastic coefficients),  
 284 i.e. the matrix representation of  $\hat{\mathcal{C}}$  (in Voigt notation) is

$$[\hat{\mathcal{C}}] = \begin{pmatrix} \hat{\mathcal{C}}_{11} & \hat{\mathcal{C}}_{12} & \hat{\mathcal{C}}_{13} & 0 & 0 & 0 \\ \hat{\mathcal{C}}_{12} & \hat{\mathcal{C}}_{11} & \hat{\mathcal{C}}_{13} & 0 & 0 & 0 \\ \hat{\mathcal{C}}_{13} & \hat{\mathcal{C}}_{13} & \hat{\mathcal{C}}_{33} & 0 & 0 & 0 \\ 0 & 0 & 0 & \hat{\mathcal{C}}_{44} & 0 & 0 \\ 0 & 0 & 0 & 0 & \hat{\mathcal{C}}_{44} & 0 \\ 0 & 0 & 0 & 0 & 0 & \hat{\mathcal{C}}_{66} \end{pmatrix}. \quad (30)$$

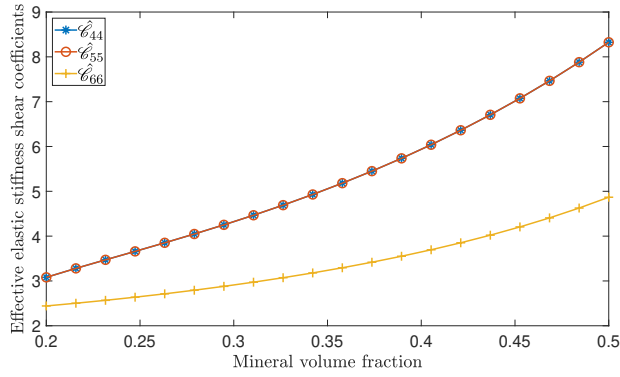


Figure 6: Shear effective elastic stiffness coefficients plotted with respect to the mineral volume fraction.

285 We now turn the attention to the computation of the effective Young's modulus ( $\hat{E}$ ), shear modulus  
 286 ( $\hat{\nu}$ ) and Poisson's ratio ( $\hat{\nu}$ ) of the hierarchical composite tissue. In particular, the effective shear modulus  
 287 for hierarchical fiber-reinforced composites has been recently studied in the previous work [47]. Here, we  
 288 adapt the computational scheme developed therein to the present framework. In the present study, via the  
 289 homogenization process, the resulting homogenized mineralized tissue shows characteristics of a tetragonal  
 290 material. Therefore, using Voigt notation, we have that

$$\hat{E}_1 = \frac{\Delta}{(\hat{\mathcal{C}}_{23})^2 - \hat{\mathcal{C}}_{22}\hat{\mathcal{C}}_{33}}, \quad \hat{\nu}_{12} = \hat{\nu}_{21} = \frac{\hat{\mathcal{C}}_{13}\hat{\mathcal{C}}_{23} - \hat{\mathcal{C}}_{12}\hat{\mathcal{C}}_{33}}{(\hat{\mathcal{C}}_{23})^2 - \hat{\mathcal{C}}_{22}\hat{\mathcal{C}}_{33}}, \quad (31a)$$

$$\hat{E}_2 = \frac{\Delta}{(\hat{\mathcal{C}}_{13})^2 - \hat{\mathcal{C}}_{11}\hat{\mathcal{C}}_{33}}, \quad \hat{\nu}_{13} = \hat{\nu}_{31} = \frac{\hat{\mathcal{C}}_{12}\hat{\mathcal{C}}_{23} - \hat{\mathcal{C}}_{13}\hat{\mathcal{C}}_{22}}{(\hat{\mathcal{C}}_{23})^2 - \hat{\mathcal{C}}_{22}\hat{\mathcal{C}}_{33}}, \quad (31b)$$

$$\hat{E}_3 = \frac{\Delta}{(\hat{\mathcal{C}}_{12})^2 - \hat{\mathcal{C}}_{11}\hat{\mathcal{C}}_{22}}, \quad \hat{\nu}_{23} = \hat{\nu}_{32} = \frac{\hat{\mathcal{C}}_{12}\hat{\mathcal{C}}_{13} - \hat{\mathcal{C}}_{11}\hat{\mathcal{C}}_{23}}{(\hat{\mathcal{C}}_{13})^2 - \hat{\mathcal{C}}_{11}\hat{\mathcal{C}}_{33}}, \quad (31c)$$

291 where

$$\Delta = (\hat{\mathcal{C}}_{13})^2\hat{\mathcal{C}}_{22} - 2\hat{\mathcal{C}}_{12}\hat{\mathcal{C}}_{13}\hat{\mathcal{C}}_{23} + \hat{\mathcal{C}}_{11}(\hat{\mathcal{C}}_{23})^2 + (\hat{\mathcal{C}}_{12})^2\hat{\mathcal{C}}_{33} - \hat{\mathcal{C}}_{11}\hat{\mathcal{C}}_{22}\hat{\mathcal{C}}_{33}. \quad (32)$$

292 Figure 7 shows the predicted effective Young's moduli (top left), shear moduli (top right) and Poisson's  
 293 ratio (bottom). We remark that it has been difficult to find experimental data measuring the anisotropic  
 294 properties of MMTs and validating the computations reported in Fig. 7. Additionally, as details regarding  
 295 the mineral content in the tissue are often not available in experimental studies, we cannot establish a logical

296 correspondence with the numerical results shown in Fig. 7, as we did previously in Fig. 5. However, in  
 297 what follows, we make a qualitative comparison with the data available in the scientific literature. In this  
 298 respect, bone has been an extensively discussed hierarchical tissue, and several experimental techniques,  
 299 such as micromechanical tests or nanoindentation [63], have been used in the measurement of its mechanical  
 300 properties. For instance, the experimental studies conducted in [32] for bone tissues show that the magnitude  
 301 of Young's and shear moduli increase with the degree of mineralization. This trend is captured by our  
 302 computations as shown in Fig. 7 (top left and top right panels). In addition, Young's moduli and Poisson's  
 303 ratio of single trabeculae in three orthogonal material directions were measured in [25] using compression  
 304 tests. Therein, it was reported Young's modulus values in the trabeculae longitudinal direction significantly  
 305 higher than those on the transverse directions. This experimental findings are in agreement with the predicted  
 306 results from the present theoretical approach as shown in Fig. 7 (top left panel). Moreover, the data collected  
 307 in the review paper [63] shows Young's modulus of trabecular bone varying between 0 Gpa ando 25 Gpa (see  
 308 Fig. 5 in [63]), which is in the range of the results obtained for low mineral concentrations. Finally, we  
 309 observe that  $\hat{\nu}_{12}$  decreases, and that  $\hat{\nu}_{13} = \hat{\nu}_{23}$  increases, with the augment of tissue's mineralization.

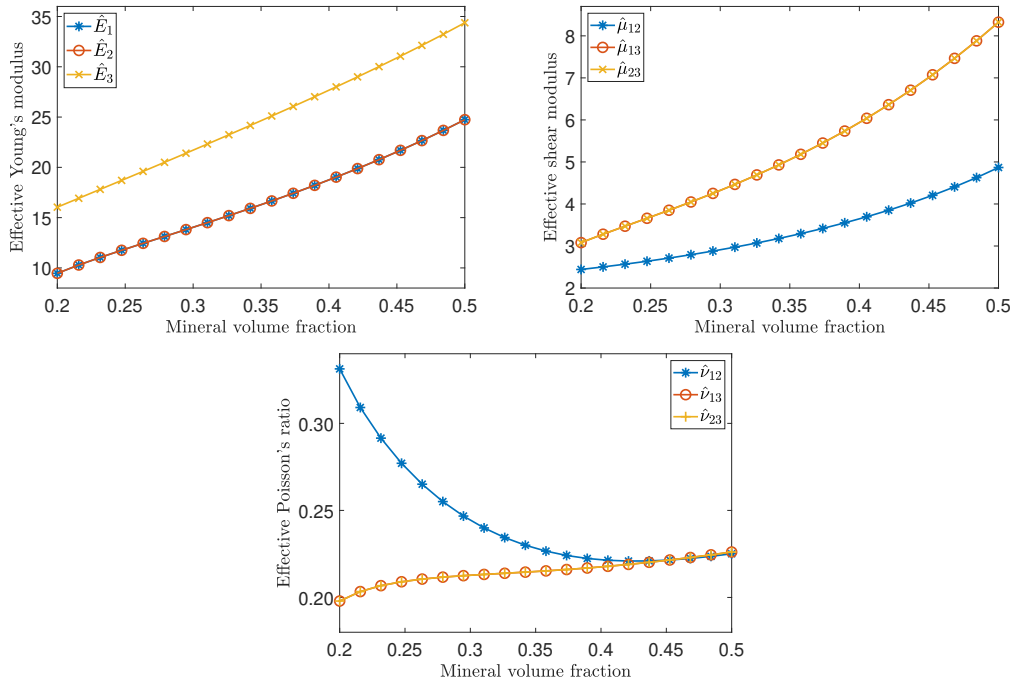


Figure 7: Comparison of the predicted effective Young's modulus, shear modulus and Poisson's ratio of the musculoskeletal mineralized tissue with respect to the mineral volume fraction. (Top)  $\hat{E}_1$ ,  $\hat{E}_2$  and  $\hat{E}_3$ , (middle)  $\hat{\mu}_{12}$ ,  $\hat{\mu}_{13}$  and  $\hat{\mu}_{23}$ , (bottom)  $\hat{\nu}_{12}$ ,  $\hat{\nu}_{13}$  and  $\hat{\nu}_{23}$ .

## 310 6 Conclusions

311 In the present work we have depicted a three-scale asymptotic homogenization procedure to investigate the  
 312 effective properties of multiscale, linear elastic composite materials. Using this approach we compute the  
 313 effective properties of a linear elastic, fiber reinforced hierarchical material using an analytical resolution  
 314 process, allowing us to reduce the computational cost necessary to calculate the homogenized properties.  
 315 Furthermore, the three-scale scheme was employed in a biological scenario of interest, that is, the modeling

316 of the macroscopic properties of MMTs. Specifically, we conducted a parametric study by varying the min-  
 317 eralization of the heterogeneous tissue, and we compared the effective axial and transverse elastic stiffnes  
 318 constants with theoretical and experimental values. In the study, we take advantage of Reuss’ lower formula  
 319 to model the properties of the extrafibrillar space. In this sense, we hypothesize that performing an asymp-  
 320 totic homogenization approach to describe the extrafibrillar space will produce more accurate outcomes for  
 321 the description of MMTs. Finally, we computed the effective Young’s and shear moduli, and Poisson’s ratio,  
 322 and we showed that the predictions are consistent with experimental findings concerning bone tissues.

323 Minerals content can substantially affect the macroscopic tissue behavior [37, 41, 18]. To avoid modeling  
 324 the complex interplay between mineral crystals and water, we embrace a simplified approach by modeling  
 325 the effective behavior of the extrafibrillar space by means of Reuss’ lower-bound formula. In this direction,  
 326 we aim to account for another scale in the homogenization process, and to solve the related local problem by  
 327 means of the finite elements method [41]. Further developments of this work include: (i) the generalization  
 328 to a nonlinear framework (e.g. considering hyperelasticity) [46, 11, 49] and (ii) the consideration of growth  
 329 of the tissue and remodelling of its internal structure [56, 44, 38, 12, 11, 49]. Another issue that could  
 330 arise in our formulation is that of a non-macroscopically uniform medium. In other words, a medium in  
 331 which the periodic cells are not independent of the macroscale and thus, the geometry can be varying  
 332 over the multiple scales, not only the elastic constants. In this particular case, the generalized Reynold’s  
 333 transport theorem (see e.g. [24]) has to be enforced as done, for instance in [40] and in [39] in the context  
 334 of poro-mechanics. Alternative approaches that are rapidly emerging in the literature also involve a more  
 335 explicit definition of the normal vector [9], which has been used to investigate the role of porosity gradients  
 336 to optimize filter efficiency [15]. Also, the macroscopic uniformity assumption may also not be suitable  
 337 for modelling peculiar situations, such as, for example, localized deformations and damage phenomena  
 338 that can violate the periodicity constraint. In this context, hierarchical computational schemes have been  
 339 developed for overcoming this issue [65, 17, 19]. In an idealized setting, one may think of reinterpreting the  
 340 small parameter  $\varepsilon_2$  as e.g. the damage length-scale and perform an analytical three-scale homogenization  
 341 approach.

342 Finally, we remark that the technique has the advantage of reducing the intrinsic geometrical complexities  
 343 when studying heterogeneous materials, and it ciphers the constituent’s properties at the several scales in  
 344 the effective coefficients.

## 345 Acknowledgement

346 ART gratefully acknowledges the research project “Mathematical multi-scale modeling of biological tissues”  
 347 (N. 64) financed by the Politecnico di Torino (Scientific Advisor: Alfio Grillo). ART and AG acknowledge  
 348 the Dipartimento di Scienze Matematiche (DISMA) “G.L. Lagrange” of the Politecnico di Torino, “Diparti-  
 349 mento di Eccellenza 2018–2022” (“Department of Excellence 2018–2022”). RRR acknowledges the funding of  
 350 Proyecto Nacional de Ciencias Básicas 2016–2018 (Project No. 7515) and to Departamento de Matemáticas  
 351 y Mecánica, IIMAS and PREI-DGAPA at UNAM.

## 352 A Solution of the cell problems

353 Following the procedure given in [45, 52, 54, 8], we present an analytical approach to find the solution of  
 354 the cell problems  $\mathcal{P}_\alpha^{qq}$  ( $q = 1, 2, 3$ ) and  $\mathcal{P}_\alpha^{12}$ . In particular, the choice of the microstructure and material  
 355 symmetry allow us to focus on only one hierarchical level.

### 356 A.1 Theoretical background

357 In the present section we list some theoretical results that will be useful in the remainder of the text.

358 **Definition 1** Let  $w_1$  and  $w_2$  two linearly independent complex numbers on  $\mathbb{R}$ , i.e., there exists no pair of  
359 real numbers  $a$  and  $b$ , with  $a, b \neq 0$ , such that  $aw_1 + bw_2 = 0$ . We define a lattice, the set of all complex  
360 numbers of the form

$$w = mw_1 + nw_2, \quad m, n \in \mathbb{Z}, \quad (33)$$

361 which is denoted by  $L = [w_1, w_2]$ .

362 **Proposition 1** The Laurent series expansion of the  $(k-1)$ -th ( $k = 2, 3, \dots$ ) derivative of Weierstrass'  
363 function ( $\zeta$ ) and Natanzon's function ( $Q$ ) in zero are, respectively,

$$\zeta^{(k-1)}(z) = \frac{(k-1)!}{z^k} - (k-1)! \sum_{l=1}^{\infty o} \Delta_{kl} z^l \quad \text{and} \quad Q^{(k-1)}(z) = (k-1)! \sum_{l=1}^{\infty o} \mathring{\Delta}_{kl} z^l, \quad (34a)$$

364 where

$$\Delta_{kl} = -\binom{k+l-1}{l} S_{k+l} \quad \text{and} \quad \mathring{\Delta}_{kl} = k \binom{k+l}{l} T_{k+l}. \quad (35)$$

365 The superscript "o" over the sum operator indicates that the sum is carried out only over odd natural  
366 numbers. The reticulate sums (which contains the geometrical information of the problem) are defined by  
367  $S_{k+l} = \sum_{w \in L^*} \frac{1}{w^{k+l}}$  ( $k+l \geq 2$ ) and  $T_{k+l} = \sum_{w \in L^*} \frac{\bar{w}}{w^{k+l+1}}$  ( $k+l \geq 3$ ). The series  $S_{k+l}$  vanishes when  $k+l$   
368 is not a multiple of 4. Furthermore, the series  $T_{k+l}$  vanishes when  $k+l$  is not of the form  $4t-1$  for  $t \in \mathbb{N}$   
369 [20]. Moreover,  $L^*$  represents the lattice excluding the number  $w = 0$  and  $\bar{w}$  denotes the conjugate of the  
370 complex number  $w$ .

371 **Proposition 2** Weierstrass' function and Natanzon's function possess the following properties of quasi-  
372 periodicity [36]

$$\zeta(z + w_p) - \zeta(z) = \delta_p, \quad \zeta^{(k)}(z + w_p) - \zeta^{(k)}(z) = 0, \quad \forall k \geq 1 \quad (36a)$$

$$Q(z + w_p) - Q(z) = \bar{w}_p P(z) + \xi_p, \quad Q^{(k)}(z + w_p) - Q^{(k)}(z) = \bar{w}_p P^{(k)}(z), \quad \forall k \geq 1, \quad (36b)$$

373 where  $P(z) = -\zeta'(z)$ ,  $\delta_p = 2\zeta(w_p/2)$  and  $\xi_p = 2Q(w_p/2) - \bar{w}_p P(w_p/2)$ . Moreover, Legendre's relations are  
374 fulfilled, i.e.,

$$\delta_1 w_2 - \delta_2 w_1 = 2\pi i, \quad (37a)$$

$$\delta_1 \bar{w}_2 - \delta_2 \bar{w}_1 = \xi_2 w_1 - \xi_1 w_2. \quad (37b)$$

375 **Remark 1** In the case of a square array of periodic cells, that is, for  $w_1 = 1$  and  $w_2 = i$ , we have that  
376  $\delta_1 = \pi$ ,  $\delta_2 = -i\pi$ ,  $\xi_1 = -\frac{5S_4}{\pi}$  and  $\xi_2 = i\frac{5S_4}{\pi}$ .

## 377 A.2 Solution of the in-plane cell problems $\mathcal{P}^{qq}$

378 The structure of the in-plane cell problems  $\mathcal{P}^{qq}$  ( $q = 1, 2, 3$ ) given in (20a) is of plane-strain and therefore,  
379 the theory of harmonic functions and the Kolosov-Muskhelishvili complex potentials [57] are applicable  
380 [45, 52, 54, 8]. The Kolosov-Muskhelishvili complex potentials are related to  $\omega_{1qq}$  and  $\omega_{2qq}$ , and to the stress  
381 components by means of the formulae,

$$2\mathcal{E}_{1212}^\gamma (\omega_{1qq}^\gamma + i\omega_{2qq}^\gamma) = \chi^\gamma \varphi^{qq\gamma} - z(\overline{\varphi^{qq\gamma}})' - \bar{\psi}^\gamma, \quad (38a)$$

$$\sigma_{11}^{qq\gamma} + \sigma_{22}^{qq\gamma} = 2((\varphi^{qq\gamma})' + (\overline{\varphi^{qq\gamma, \alpha}})'), \quad (38b)$$

$$\sigma_{22}^{qq\gamma} - \sigma_{11}^{qq\gamma} = 2(\bar{z}(\varphi^{qq\gamma})'' + (\psi^{qq\gamma})'), \quad (38c)$$



382 where  $\chi^\gamma = 3 - 4\nu^\gamma$  and  $\nu^\gamma = \mathcal{C}_{1122}^\gamma / (\mathcal{C}_{1111}^\gamma + \mathcal{C}_{1122}^\gamma)$ . The notation  $\varphi'$  indicates the derivative of  $\varphi$  with  
 383 respect to the complex variable  $z$ . Following [45, 52, 54, 8], the complex potentials  $\varphi^{qq\gamma}$  and  $\psi^{qq\gamma}$  can be  
 384 written as

$$\varphi^{qqm}(z) = \frac{a_0^{qq}}{R}z + \sum_{k=1}^{\infty o} a_k^{qq} R^k \frac{\zeta^{(k-1)}(z)}{(k-1)!}, \quad \varphi^{qqf}(z) = \sum_{k=1}^{\infty o} \frac{z^k}{R^k} c_k^{qq}, \quad (39a)$$

$$\psi^{qqm}(z) = \frac{b_0^{qq}}{R}z + \sum_{k=1}^{\infty o} b_k^{qq} R^k \frac{\zeta^{(k-1)}(z)}{(k-1)!} + \sum_{k=1}^{\infty o} a_k^{qq} R^k \frac{Q^{(k-1)}(z)}{(k-1)!}, \quad \psi^{qqf}(z) = \sum_{k=1}^{\infty o} \frac{z^k}{R^k} d_k^{qq}, \quad (39b)$$

385 where  $a_k^{qq}$ ,  $b_k^{qq}$  ( $k = 0, 1, 3, \dots$ ), and  $c_k^{qq}$ ,  $d_k^{qq}$  ( $k = 1, 3, \dots$ ) are complex coefficients to be determined. The  
 386 radius of the fiber's circular cross section is denoted with  $R$ .

387 Using Proposition 1 the complex potentials  $\varphi^{qqm}$  and  $\psi^{qqm}$  can be rewritten as follows

$$\varphi^{qqm}(z) = \frac{a_0^{qq}}{R}z + \sum_{l=1}^{\infty o} \left( a_l^{qq} \frac{R^l}{z^l} + A_l^{qq} \frac{z^l}{R^l} \right), \quad (40a)$$

$$\psi^{qqm}(z) = \frac{b_0^{qq}}{R}z + \sum_{l=1}^{\infty o} \left( b_l^{qq} \frac{R^l}{z^l} + B_l^{qq} \frac{z^l}{R^l} + \mathring{A}_l^{qq} \frac{z^l}{R^l} \right), \quad (40b)$$

388 where  $A_l^{qq} = \sum_{k=1}^{\infty o} \Lambda_{kl} a_k^{qq}$ ,  $B_l^{qq} = \sum_{k=1}^{\infty o} \Lambda_{kl} b_k^{qq}$  and  $\mathring{A}_l^{qq} = \sum_{k=1}^{\infty o} \mathring{\Lambda}_{kl} a_k^{qq}$ , with  $\Lambda_{kl} = \Delta_{kl} R^{k+l}$  and  $\mathring{\Lambda}_{kl} =$   
 389  $\mathring{\Delta}_{kl} R^{k+l}$ .

390 Then, to find the solution of problem (20a) is equivalent to determine the unknowns  $a_k^{qq}$ ,  $b_k^{qq}$ ,  $c_k^{qq}$  and  
 391  $d_k^{qq}$ . In particular, we show that for computing the effective coefficients, it is sufficient to find  $a_1^{qq}$ . In the  
 392 following, we outline in three steps, the procedure in [45, 52, 54, 8].

393 **Step 1:** By taking into account the continuity conditions on  $\omega_{1qq}$  and  $\omega_{2qq}$  and the two expressions in  
 394 (38a) for  $\gamma = m$  and  $\gamma = f$ , we can deduce that

$$\chi^* (\chi^m \varphi^{qqm} - z \overline{(\varphi^{qqm})'}) - \overline{\psi^{qqm}} = \chi^f \varphi^{qqf} - z \overline{(\varphi^{qqf})'} - \overline{\psi^{qqf}}, \quad (41)$$

395 where  $\chi^* = \mathcal{C}_{1212}^f / \mathcal{C}_{1212}^m$ . Furthermore, the continuity conditions for traction on the interface  $\tilde{\Gamma} = Re^{i\theta}$ ,  
 396  $\theta \in [0, 2\pi]$ , lead us to the following relation

$$\begin{aligned} & (\sigma_{22}^{qqm} + 2i\sigma_{12}^{qqm} - \sigma_{11}^{qqm})e^{i\theta} - (\sigma_{11}^{qqm} + \sigma_{22}^{qqm})e^{-i\theta} + 2\beta_1^{qq}e^{i\theta} - 2\beta_2^{qq}e^{-i\theta} \\ & = (\sigma_{22}^{qqf} + 2i\sigma_{12}^{qqf} - \sigma_{11}^{qqf})e^{i\theta} - (\sigma_{11}^{qqf} + \sigma_{22}^{qqf})e^{-i\theta}, \end{aligned} \quad (42)$$

397 where

$$\beta_j^{qq} = \begin{cases} \frac{[\mathcal{C}_{1122}] + (-1)^j [\mathcal{C}_{1111}]}{2}, & q = 1, \\ (-1)^j \beta_j^{11}, & q = 2, \\ \frac{1 + (-1)^j}{2} [\mathcal{C}_{1133}], & q = 3, \end{cases} \quad (43)$$

398 with  $j = 1, 2$ .

399 **Step 2:** Subsequently, let us evaluate (38a) (for  $\gamma = m$ ) in  $z$  and  $z + w_p$  and subtract the results of  
 400 these evaluations. Using the expansions (40a) and (40b), the properties of quasiperiodicity (36a)–(36b), the  
 401 periodic properties of the functions involved and Legendre's relations, we obtain that

$$a_0^{qq} + \overline{a_0^{qq}} = [(\tau_2 - \chi^m \tau_1) a_1^{qq} + (\overline{\tau_2} - \chi^m \overline{\tau_1}) \overline{a_1^{qq}} + (\tau_3 + \overline{\tau_3}) b_1^{qq}] \frac{R^2}{\chi^m - 1}, \quad (44a)$$

$$a_0^{qq} - \overline{a_0^{qq}} = [-(\tau_2 + \chi^m \tau_1) a_1^{qq} + (\overline{\tau_2} + \chi^m \overline{\tau_1}) \overline{a_1^{qq}} - (\tau_3 - \overline{\tau_3}) b_1^{qq}] \frac{R^2}{\chi^m - 1}, \quad (44b)$$

$$\overline{b_0^{qq}} = (\tau_4 \chi^m a_1^{qq} + \overline{\tau_5 a_1^{qq}} - \overline{\tau_6 b_1^{qq}}) R^2, \quad (44c)$$

402 where

$$\tau_1 = (\overline{w_1} \delta_2 - \overline{w_2} \delta_1) / W, \quad \tau_4 = -(w_1 \delta_2 - w_2 \delta_1) / W, \quad (45a)$$

$$\overline{\tau_2} = (\overline{w_1} \xi_2 - \overline{w_2} \xi_1) / W, \quad \overline{\tau_5} = (w_1 \overline{\xi_2} - w_2 \overline{\xi_1}) / W, \quad (45b)$$

$$\overline{\tau_3} = (\overline{w_1} \delta_2 - \overline{w_2} \delta_1) / W, \quad \overline{\tau_6} = -(w_1 \overline{\delta_2} - w_2 \overline{\delta_1}) / W, \quad (45c)$$

403 where  $W = \overline{w_1} w_2 - w_1 \overline{w_2}$ . Furthermore, substituting the Kolosov-Muskhelishvili relationships (38b) and  
404 (38c) in equation (42), we obtain

$$z(\overline{\varphi^{qqm}})' + \overline{\psi^{qqm}} + \varphi^{qqm} + \overline{z} \beta_1^{qq} + z \beta_2^{qq} = z(\overline{\varphi^{qqf}})' + \overline{\psi^{qqf}} + \varphi^{qqf}. \quad (46)$$

405 **Step 3:** Now, substituting the Laurent expansions (40a) and (40b) in (41) and in (46), we obtain the  
406 following infinite linear system in the unknowns  $\tilde{a}_l^{qq} = a_l^{qq} / (R \beta_2^{qq})$  ( $q = 1, 2, 3$  and  $l = 1, 3, 5, \dots$ )

$$\tilde{a}_l^{qq} + \mathcal{H}_l^1 \tilde{a}_1^{qq} + \mathcal{H}_l^2 \overline{\tilde{a}_1^{qq}} + \sum_{k=1}^{\infty} \mathcal{W}_{kl} \tilde{a}_k^{qq} + \sum_{k=1}^{\infty} \mathcal{M}_{kl} \overline{\tilde{a}_k^{qq}} = \mathcal{H}_l^{qq}, \quad (47)$$

407 where

$$\mathcal{H}_l^1 = [2\tau_4 \chi^m (\chi^m - 1) \chi^{m*} R^2 \delta_{1l} + (\overline{\Lambda_{1l}} - \overline{\tau_6} R^2 \delta_{1l}) (\tau_2 - \chi^m \tau_1) \Upsilon R^2] / [2(\chi^m - 1)], \quad (48a)$$

$$\mathcal{H}_l^2 = [2\overline{\tau_5} (\chi^m - 1) \chi^{m*} R^2 \delta_{1l} + (\overline{\Lambda_{1l}} - \overline{\tau_6} R^2 \delta_{1l}) (\overline{\tau_2} - \chi^m \overline{\tau_1}) \Upsilon R^2] / [2(\chi^m - 1)], \quad (48b)$$

$$\mathcal{W}_{kl} = \chi^{mf*} \mathcal{V}_{kl} + \frac{1}{2} (\overline{\Lambda_{1l}} - \overline{\tau_6} R^2 \delta_{1l}) \Upsilon \Lambda_{k1}, \quad (48c)$$

$$\mathcal{M}_{kl} = \chi^{m*} \mathcal{N}_{kl} + \frac{1}{2} (\overline{\Lambda_{1l}} - \overline{\tau_6} R^2 \delta_{1l}) \Upsilon \overline{\Lambda_{k1}}, \quad (48d)$$

$$\mathcal{N}_{kl} = (l+2) \overline{\Lambda_{k(l+2)}} + k \overline{\Lambda_{(k+2)l}} + \overline{\Lambda_{kl}}, \quad (48e)$$

$$\mathcal{V}_{kl} = \sum_{j=1}^{\infty} \Lambda_{k(j+2)} \overline{\Lambda_{(j+2)l}}, \quad (48f)$$

$$\mathcal{H}_l^{qq} = (\theta \beta_1^{qq} / \beta_2^{qq} - \overline{\tau_6} R^2 \Upsilon^*) \delta_{1l} + \overline{\Lambda_{1l}} \Upsilon^*, \quad (48g)$$

$$\alpha_0 = \chi^* [1 - Re(\tau_3) R^2] + (\chi^f - 1) \left[ \frac{Re(\tau_3) R^2}{\chi^m - 1} + \frac{1}{2} \right], \quad (48h)$$

$$\theta = -(\chi^* \chi^m + 1)^{-1}, \quad (48i)$$

$$\chi^{m*} = (1 - \chi^*) (\chi^* \chi^m + 1)^{-1}, \quad (48j)$$

$$\chi^{mf*} = (\chi^{m*} (\chi^* \chi^m - \chi^f)) (\chi^* + \chi^f)^{-1}, \quad (48k)$$

$$\Upsilon = (\chi^{m*} (1 + \chi^* \chi^m - \chi^* - \chi^f)) \alpha_0^{-1}, \quad (48l)$$

$$\Upsilon^* = (\chi^{m*} (\chi^f - 1)) (2\alpha_0)^{-1}. \quad (48m)$$

408 In particular, the linear system (47) can be equivalently rewritten as

$$\begin{pmatrix} \tilde{A}_r^{qq} \\ \tilde{A}_i^{qq} \end{pmatrix} = \begin{pmatrix} \mathcal{I} + \check{\mathcal{M}}_r + \check{\mathcal{W}}_r & \check{\mathcal{M}}_i - \check{\mathcal{W}}_i \\ \check{\mathcal{M}}_i + \check{\mathcal{W}}_i & \mathcal{I} + \check{\mathcal{M}}_r - \check{\mathcal{W}}_r \end{pmatrix}^{-1} \begin{pmatrix} \mathcal{H}_r^{qq} \\ \mathcal{H}_i^{qq} \end{pmatrix}, \quad (49)$$

409 where  $\tilde{\mathcal{A}}_r^{qq} = (Re(\tilde{a}_1^{qq}), Re(\tilde{a}_3^{qq}), \dots)^T$ ,  $\tilde{\mathcal{A}}_i^{qq} = (Im(\tilde{a}_1^{qq}), Im(\tilde{a}_3^{qq}), \dots)^T$ , with  $\mathbf{a}^T$  denoting the operation of  
410 transposition of the vector  $\mathbf{a}$ . Moreover,  $\mathcal{I}$  is the infinite identity matrix,  $\check{\mathcal{M}}_r = Re(\check{\mathcal{M}})$ ,  $\check{\mathcal{W}}_r = Re(\check{\mathcal{W}})$ ,  
411  $\check{\mathcal{M}}_i = Im(\check{\mathcal{M}})$ ,  $\check{\mathcal{W}}_i = Im(\check{\mathcal{W}})$ ,  $\mathcal{H}_r^{qq} = Re(\mathcal{H}^{qq})$  and  $\mathcal{H}_i^{qq} = Im(\mathcal{H}^{qq})$ , where  $Re(\Phi)$  and  $Im(\Phi)$  denote  
412 the operators that extract the real and imaginary parts of  $\Phi$ , respectively. The matrices  $\check{\mathcal{M}}$  and  $\check{\mathcal{W}}$  are  
413 decomposed additively as follows,  $\check{\mathcal{M}} = \mathcal{U} + \mathcal{M}$  and  $\check{\mathcal{W}} = \mathcal{Q} + \mathcal{W}$ , where the components of  $\mathcal{U}$  and  $\mathcal{Q}$ , are  
414 given by the following expressions,

$$U_{kl} = \begin{cases} [2\tau_4\chi^m(\chi^m - 1)\chi^{m*}R^2\delta_{1l} + (\overline{\Lambda_{11}} - \overline{\tau_6}R^2\delta_{1l})(\tau_2 - \chi^m\tau_1)\Upsilon R^2][2(\chi^m - 1)]^{-1}, & k = 1, \\ 0, & k > 1, \end{cases} \quad (50a)$$

$$Q_{kl} = \begin{cases} [2\overline{\tau_5}(\chi^m - 1)\chi^{m*}R^2\delta_{1l} + (\overline{\Lambda_{11}} - \overline{\tau_6}R^2\delta_{1l})(\overline{\tau_2} - \chi^m\overline{\tau_1})\Upsilon R^2][2(\chi^m - 1)]^{-1}, & k = 1, \\ 0, & k > 1. \end{cases} \quad (50b)$$

415 Equation (49) is an infinite linear system with an infinite number of unknowns for which is possible to  
416 obtain a solution by truncation through a convergent sequence of solutions [27, 52, 54, 8].

### 417 A.3 Solution of the problem $\mathcal{P}^{12}$

418 The solution of the in-plane problem  $\mathcal{P}^{12}$  (20b) can be found following a similar procedure to the one  
419 outlined above. In such a case, the following infinite linear system in the unknowns  $\tilde{a}_l^{12}$  ( $l = 1, 3, 5, \dots$ ) is  
420 obtained

$$\begin{pmatrix} \tilde{\mathcal{A}}_r^{12} \\ \tilde{\mathcal{A}}_i^{12} \end{pmatrix} = \begin{pmatrix} \mathcal{I} + \check{\mathcal{M}}_r + \check{\mathcal{W}}_r & \check{\mathcal{M}}_i - \check{\mathcal{W}}_i \\ \check{\mathcal{M}}_i + \check{\mathcal{W}}_i & \mathcal{I} + \check{\mathcal{M}}_r - \check{\mathcal{W}}_r \end{pmatrix}^{-1} \begin{pmatrix} \mathcal{H}_r^{12} \\ \mathcal{H}_i^{12} \end{pmatrix}, \quad (51)$$

421 where  $\tilde{\mathcal{A}}_r^{12} = (Re(\tilde{a}_1^{12}), Re(\tilde{a}_3^{12}), \dots)^T$ ,  $\tilde{\mathcal{A}}_i^{12} = (Im(\tilde{a}_1^{12}), Im(\tilde{a}_3^{12}), \dots)^T$ ,  $\mathcal{H}_l^{12} = -i\theta\delta_{1l}$  and  $\tilde{a}_l^{12} = a_l^{12}/(R[\mathcal{C}_{1212}])$ .

## 422 B Effective coefficients

423 The fact that  $\mathcal{C}^{\varepsilon_2}$  is isotropic, together with the assumption that the cell's cross section corresponds to a  
424 square embedding a single circle, induce that the tensor  $\mathcal{C}$  has tetragonal symmetric structure. This result  
425 together with the isotropy assumption of the constituent  $\Omega_m^{\varepsilon_1}$  imply that the effective tensor  $\hat{\mathcal{C}}$  is at most  
426 monoclinic, that is,  $\hat{\mathcal{C}}$  has at most 13 independent effective elastic coefficients. In the following, we will  
427 consider two elasticity tensors  $\mathcal{C}^m$  and  $\mathcal{C}^f$  having tetragonal symmetric structure. In this way, the results  
428 will apply to both hierarchical levels.

### 429 B.1 The in-plane effective coefficients

430 Taking into account the major and minor symmetries of the elasticity tensor, the non-zero effective coefficients  
431 corresponding to the in-plane problems  $\mathcal{P}^{qq}$  are

$$\hat{\mathcal{C}}_{11qq} = \langle \mathcal{C}_{1111}^{\varepsilon} \frac{\partial \omega_{1qq}}{\partial y_1} + \mathcal{C}_{1122}^{\varepsilon} \frac{\partial \omega_{2qq}}{\partial y_2} + \mathcal{C}_{11qq}^{\varepsilon} \rangle, \quad (52a)$$

$$\hat{\mathcal{C}}_{12qq} = \langle \mathcal{C}_{1221}^{\varepsilon} \frac{\partial \omega_{2qq}}{\partial y_1} + \mathcal{C}_{1212}^{\varepsilon} \frac{\partial \omega_{1qq}}{\partial y_2} \rangle, \quad (52b)$$

$$\hat{\mathcal{C}}_{21qq} = \langle \mathcal{C}_{2121}^{\varepsilon} \frac{\partial \omega_{2qq}}{\partial y_1} + \mathcal{C}_{2112}^{\varepsilon} \frac{\partial \omega_{1qq}}{\partial y_2} \rangle, \quad (52c)$$

$$\hat{\mathcal{C}}_{22qq} = \langle \mathcal{C}_{2211}^{\varepsilon} \frac{\partial \omega_{1qq}}{\partial y_1} + \mathcal{C}_{2222}^{\varepsilon} \frac{\partial \omega_{2qq}}{\partial y_2} + \mathcal{C}_{22qq}^{\varepsilon} \rangle, \quad (52d)$$

$$\hat{\mathcal{C}}_{33qq} = \langle \mathcal{C}_{3311}^\varepsilon \frac{\partial \omega_{1qq}}{\partial y_1} + \mathcal{C}_{3322}^\varepsilon \frac{\partial \omega_{2qq}}{\partial y_2} + \mathcal{C}_{33qq}^\varepsilon \rangle. \quad (52e)$$

432 We observe that the variable  $y$  plays the role of  $\eta$  and  $\varsigma$  since the procedure to obtain the effective coefficients,  
433 for this particular case, is the same.

434 Working with the expressions (52a)–(52e), applying Green's theorem to find the integrals involved, taking  
435 into account the periodicity properties of the involved functions, the continuity conditions on the interface  
436  $\tilde{\Gamma}$ , the Kolosov-Muskhelishvili formula (38a), the Laurent expansions of  $\varphi^{qqm}$  and  $\psi^{qqm}$ , the orthogonality  
437 property of the system of functions  $\{e^{in\theta}\}_{n=-\infty}^{+\infty}$  in the interval  $[-\pi, \pi]$ , we can write

$$\begin{aligned} \hat{\mathcal{C}}_{11qq} = & \langle \mathcal{C}_{11qq} \rangle - V_f \beta_2^{qq} [\beta_2^{11} [2\chi^* \chi^{m*} (\chi^f + 1) \mathcal{C}_{1212}^m]^{-1} Re(\chi^f \Xi^{qq} - \overline{\Xi^{qq}}) \\ & + Re((\chi^m + 1) \overline{a_1^{qq}} + \beta_1^{qq} (\beta_2^{qq})^{-1})], \end{aligned} \quad (53a)$$

$$\begin{aligned} \hat{\mathcal{C}}_{22qq} = & \langle \mathcal{C}_{22qq} \rangle - V_f \beta_2^{qq} [\beta_2^{11} [2\chi^* \chi^{m*} (\chi^f + 1) \mathcal{C}_{1212}^m]^{-1} Re(\chi^f \Xi^{qq} - \overline{\Xi^{qq}}) \\ & - Re((\chi^m + 1) \overline{a_1^{qq}} + \beta_1^{qq} (\beta_2^{qq})^{-1})], \end{aligned} \quad (53b)$$

$$\hat{\mathcal{C}}_{33qq} = \langle \mathcal{C}_{33qq} \rangle - V_f \beta_2^{33} \beta_2^{qq} [2\chi^* \chi^{m*} (\chi^f + 1) [\mathcal{C}_{1212}^m]^{-1} Re(\chi^f \Xi^{qq} - \overline{\Xi^{qq}})], \quad (53c)$$

$$\hat{\mathcal{C}}_{12qq} = V_f \beta_2^{qq} Im((\chi^m + 1) \overline{a_1^{qq}} + \beta_1^{qq} (\beta_2^{qq})^{-1}), \quad (53d)$$

438 where  $V_f = \pi R^2$  represents the volume fraction of the circular inclusion and

$$\begin{aligned} \Xi^{qq} = & \{[(\chi^{m*} \chi_-^m + \Upsilon \beta_0) \tau_2 - (\chi^{m*} \chi_-^* + \Upsilon \beta_0) \tau_1 \chi^m] R^2\} (\chi^m - 1)^{-1} \overline{a_1^{qq}} + \{[(\chi^{m*} \chi_-^* + \Upsilon \beta_0) \overline{\tau_2} \\ & - (\chi^{m*} \chi_-^m + \Upsilon \beta_0) \overline{\tau_1} \chi^m] R^2\} (\chi^m - 1)^{-1} \overline{a_1^{qq}} + (\chi^{m*} \chi_+ + \Upsilon \beta_0) \tilde{A}_1^{qq} + (\chi^{m*} \chi_- + \Upsilon \beta_0) \overline{\tilde{A}_1^{qq}} \\ & + \chi^{m*} (\chi^f + 1) - 2\beta_0 \Upsilon^*, \end{aligned} \quad (54a)$$

$$\beta_0 = (\chi^f + 1) \left[ \frac{Re(\tau_3) R^2}{\chi^m - 1} + \frac{1}{2} \right] - i \chi^* Im(\tau_3) R^2, \quad (54b)$$

$$\chi_-^m = \chi^f + 1 - \chi^* \chi^m + \chi^*, \quad (54c)$$

$$\chi_-^* = \chi^f + 1 + \chi^* \chi^m - \chi^*, \quad (54d)$$

$$\chi_+ = \chi^f + 1 + \chi^* \chi^m + \chi^*, \quad (54e)$$

$$\chi_- = \chi^f + 1 - \chi^* \chi^m - \chi^*. \quad (54f)$$

439 In (54a), we denote by  $\tilde{A}_l^{qq} = \sum_{k=1}^{\infty} \Lambda_{kl} \tilde{a}_l^{qq}$ .

440 Resuming, formulae (53a), (53b), (53c) and (53d) give the effective coefficients  $\hat{\mathcal{C}}_{11qq}$ ,  $\hat{\mathcal{C}}_{22qq}$ ,  $\hat{\mathcal{C}}_{33qq}$  and  
441  $\hat{\mathcal{C}}_{12qq}$ , respectively. As anticipated, the effective coefficients depend solely on the unknowns  $a_1^{qq}$ .

442 Finally, proceeding in an analogous way, the only one non-zero effective coefficient corresponding to the  
443 in-plane problem  $\mathcal{P}^{12}$  is

$$\hat{\mathcal{C}}_{1212} = \mathcal{C}_{1212}^m - \llbracket \mathcal{C}_{1212} \rrbracket V_f Im((\chi^m + 1) \tilde{a}_1^{12}). \quad (55)$$

## 444 References

- 445 [1] B. Alexander, T. L. Daulton, G. M. Genin, J. Lipner, J. D. Pasteris, B. Wopenka, and S. Thomopoulos.  
446 The nanometre-scale physiology of bone: steric modelling and scanning transmission electron microscopy  
447 of collagen-mineral structure. *Journal of The Royal Society Interface*, 9(73):1774–1786, feb 2012.
- 448 [2] G. Allaire and M. Briane. Multiscale convergence and reiterated homogenisation. *Proceedings of the*  
449 *Royal Society of Edinburgh: Section A Mathematics*, 126(02):297–342, jan 1996.
- 450 [3] Jean-Louis Auriault, Claude Boutin, and Christian Geindreau, editors. *Homogenization of Coupled*  
451 *Phenomena in Heterogenous Media*. ISTE, jan 2009.

- 452 [4] Thomas K. Bader, Karin Hofstetter, Christian Hellmich, and Josef Eberhardsteiner. The poroelastic  
453 role of water in cell walls of the hierarchical composite “softwood”. *Acta Mechanica*, 217(1-2):75–100,  
454 aug 2011.
- 455 [5] Won-Gyu Bae, Hong Nam Kim, Doogon Kim, Suk-Hee Park, Hoon Eui Jeong, and Kahp-Yang Suh. 25th  
456 anniversary article: Scalable multiscale patterned structures inspired by nature: the role of hierarchy.  
457 *Advanced Materials*, 26(5):675–700, dec 2013.
- 458 [6] N. Bakhvalov and G. Panasenko. *Homogenisation: Averaging Processes in Periodic Media*. Springer  
459 Netherlands, 1989.
- 460 [7] A. Bensoussan, J. L. Lions, and G. Papanicolau. *Asymptotic Analysis for Periodic Structures*. Elsevier  
461 Science, 1978.
- 462 [8] Julián Bravo-Castillero, Raúl Guinovart-Díaz, Federico J. Sabina, and Reinaldo Rodríguez-Ramos.  
463 Closed-form expressions for the effective coefficients of a fiber-reinforced composite with transversely  
464 isotropic constituents – II. piezoelectric and square symmetry. *Mechanics of Materials*, 33(4):237–248,  
465 apr 2001.
- 466 [9] Maria Bruna and S Jonathan Chapman. Diffusion in spatially varying porous media. *SIAM Journal*  
467 *on Applied Mathematics*, 75(4):1648–1674, 2015.
- 468 [10] Doina Cioranescu and Patrizia Donato. *An Introduction to Homogenization*. Oxford University Press,  
469 1999.
- 470 [11] J. Collis, D. L. Brown, M. E. Hubbard, and R. D. O’Dea. Effective equations governing an active poroe-  
471 lastic medium. *Proceedings of the Royal Society A: Mathematical, Physical and Engineering Science*,  
472 473(2198):20160755, feb 2017.
- 473 [12] J. Collis, M.E. Hubbard, and R.D. O’Dea. Computational modelling of multiscale, multiphase fluid  
474 mixtures with application to tumour growth. *Computer Methods in Applied Mechanics and Engineering*,  
475 309:554–578, sep 2016.
- 476 [13] Stephen C. Cowin, editor. *Bone Mechanics Handbook*. CRC Press, second edition edition, 2001.
- 477 [14] J.M. Crolet, B. Aoubiza, and A. Meunier. Compact bone: Numerical simulation of mechanical charac-  
478 teristics. *Journal of Biomechanics*, 26(6):677–687, jun 1993.
- 479 [15] Mohit P Dalwadi, Ian M Griffiths, and Maria Bruna. Understanding how porosity gradients can make  
480 a better filter using homogenization theory. *Proceedings of the Royal Society A: Mathematical, Physical*  
481 *and Engineering Sciences*, 471(2182):20150464, 2015.
- 482 [16] Yu.I. Dimitrienko, I.D. Dimitrienko, and S.V. Sbornikov. Multiscale hierarchical modeling of fiber  
483 reinforced composites by asymptotic homogenization method. *Applied Mathematical Sciences*, 9:7211–  
484 7220, 2015.
- 485 [17] J Fish. Multiscale analysis of composite materials and structures. *Composites Science and Technology*,  
486 60(12-13):2547–2556, sep 2000.
- 487 [18] J. García-Rodríguez and J. Martínez-Reina. Elastic properties of woven bone: effect of mineral content  
488 and collagen fibrils orientation. *Biomechanics and Modeling in Mechanobiology*, 16(1):159–172, jul 2016.
- 489 [19] Somnath Ghosh, Kyunghoon Lee, and Prasanna Raghavan. A multi-level computational model for  
490 multi-scale damage analysis in composite and porous materials. *International Journal of Solids and*  
491 *Structures*, 38(14):2335–2385, apr 2001.
- 492 [20] E. I. Grigolyuk and L. A. Fil’shtinskii. Perforated plates and shells. *Nauka, Moscow, in Russian*, 1970.
- 493 [21] Elham Hamed, Yikhan Lee, and Iwona Jasiuk. Multiscale modeling of elastic properties of cortical  
494 bone. *Acta Mechanica*, 213(1-2):131–154, may 2010.

- 495 [22] R. Hill. Elastic properties of reinforced solids: Some theoretical principles. *Journal of the Mechanics*  
496 *and Physics of Solids*, 11(5):357–372, sep 1963.
- 497 [23] Scott J. Hollister and Cheng Yu Lin. Computational design of tissue engineering scaffolds. *Computer*  
498 *Methods in Applied Mechanics and Engineering*, 196(31-32):2991–2998, jun 2007.
- 499 [24] Mark H. Holmes. *Introduction to Perturbation Methods*. Springer New York, 2013.
- 500 [25] Junghwa Hong, H. Cha, Y. Park, S. Lee, G. Khang, and Y. Kim. Elastic moduli and poisson’s ratios  
501 of microscopic human femoral trabeculae. In T. Jarm, P. Kramar, and A. Zupanic A., editors, *11th*  
502 *Mediterranean Conference on Medical and Biomedical Engineering and Computing 2007*, volume 16 of  
503 *IFMBE Proceedings*, pages 274–277. Springer Berlin Heidelberg, 2007.
- 504 [26] Muneo Hori and Sia Nemat-Nasser. On two micromechanics theories for determining micro–macro  
505 relations in heterogeneous solids. *Mechanics of Materials*, 31(10):667–682, oct 1999.
- 506 [27] L. V. Kantorovich and V. I. Krylov. *Approximate methods of higher analysis*. Interscience Publishers,  
507 Inc., The Netherlands, 1964.
- 508 [28] Chang-Soo Kim, Charles Randow, and Tomoko Sano, editors. *Hybrid and Hierarchical Composite*  
509 *Materials*. Springer International Publishing, 2015.
- 510 [29] D. Lukkassen and G. W. Milton. On hierarchical structures and reiterated homogenization. In Michael  
511 Cwikel, Miroslav Englis, Alois Kufner, Lars-Erik Persson, and Gunnar Sparr, editors, *Function Spaces,*  
512 *Interpolation Theory and Related Topics*, pages 355–368. De Gruyter, 2002.
- 513 [30] C. C. Mei and J.-L. Auriault. Mechanics of heterogeneous porous media with several spatial scales.  
514 *Proceedings of the Royal Society A: Mathematical, Physical and Engineering Sciences*, 426(1871):391–  
515 423, dec 1989.
- 516 [31] Graeme W. Milton. *The Theory of Composites*. Cambridge University Press, 2002.
- 517 [32] Lars Mulder, Jan Harm Koolstra, Jaap MJ den Toonder, and Theo MGJ van Eijden. Relationship be-  
518 tween tissue stiffness and degree of mineralization of developing trabecular bone. *Journal of Biomedical*  
519 *Materials Research Part A*, 84A(2):508–515, jul 2008.
- 520 [33] Toshio Mura. *Micromechanics of defects in solids*. Springer Netherlands, 1987.
- 521 [34] N. I. Muskhelishvili. *Some Basic Problems of the Mathematical Theory of Elasticity*. Springer Nether-  
522 lands, 1977.
- 523 [35] Eduardo S. Nascimento, Manuel E. Cruz, and Julián Bravo-Castillero. Calculation of the effective ther-  
524 mal conductivity of multiscale ordered arrays based on reiterated homogenization theory and analytical  
525 formulae. *International Journal of Engineering Science*, 119:205–216, oct 2017.
- 526 [36] V. Ya. Natanzon. On the stresses in a plate in tension, weakened by identical holes arranged in a  
527 staggered array. *Matem.*, 1935.
- 528 [37] Svetoslav Nikolov and Dierk Raabe. Hierarchical modeling of the elastic properties of bone at submicron  
529 scales: The role of extrafibrillar mineralization. *Biophysical Journal*, 94(11):4220–4232, jun 2008.
- 530 [38] R. D. O’Dea, M. R. Nelson, A. J. El Haj, S. L. Waters, and H. M. Byrne. A multiscale analysis of nutrient  
531 transport and biological tissue growth in vitro. *Mathematical Medicine and Biology*, 32(3):345–366, oct  
532 2014.
- 533 [39] R. Penta, D. Ambrosi, and A. Quarteroni. Multiscale homogenization for fluid and drug transport in  
534 vascularized malignant tissues. *Mathematical Models and Methods in Applied Sciences*, 25(01):79–108,  
535 jan 2015.
- 536 [40] R. Penta, D. Ambrosi, and R. J. Shipley. Effective governing equations for poroelastic growing media.  
537 *The Quarterly Journal of Mechanics and Applied Mathematics*, 67(1):69–91, jan 2014.

- 538 [41] R Penta, K Raum, Q Grimal, S Schrof, and A Gerisch. Can a continuous mineral foam explain the  
539 stiffening of aged bone tissue? a micromechanical approach to mineral fusion in musculoskeletal tissues.  
540 *Bioinspiration & Biomimetics*, 11(3):035004, may 2016.
- 541 [42] Raimondo Penta and Alf Gerisch. Investigation of the potential of asymptotic homogenization for elastic  
542 composites via a three-dimensional computational study. *Computing and Visualization in Science*,  
543 17(4):185–201, aug 2015.
- 544 [43] Raimondo Penta and Alf Gerisch. The asymptotic homogenization elasticity tensor properties for  
545 composites with material discontinuities. *Continuum Mechanics and Thermodynamics*, 29(1):187–206,  
546 aug 2017.
- 547 [44] Malte A. Peter. Coupled reaction–diffusion processes inducing an evolution of the microstructure:  
548 Analysis and homogenization. *Nonlinear Analysis: Theory, Methods & Applications*, 70(2):806–821,  
549 jan 2009.
- 550 [45] B. E. Pobedrya. *Mechanics of composite materials*. Moscow State University Press, Moscow, in Russian,  
551 1984.
- 552 [46] E. Pruchnicki. Hyperelastic homogenized law for reinforced elastomer at finite strain with edge effects.  
553 *Acta Mechanica*, 129(3-4):139–162, sep 1998.
- 554 [47] Ariel Ramírez-Torres, Raimondo Penta, Reinaldo Rodríguez-Ramos, Alfio Grillo, Luigi Preziosi, José  
555 Merodio, Raúl Guinovart-Díaz, and Julián Bravo-Castillero. Homogenized out-of-plane shear response  
556 of three-scale fiber-reinforced composites. *Computing and Visualization in Science*, jun 2018.
- 557 [48] Ariel Ramírez-Torres, Raimondo Penta, Reinaldo Rodríguez-Ramos, José Merodio, Federico J. Sabina,  
558 Julián Bravo-Castillero, Raúl Guinovart-Díaz, Luigi Preziosi, and Alfio Grillo. Three scales asymptotic  
559 homogenization and its application to layered hierarchical hard tissues. *International Journal of Solids  
560 and Structures*, 130-131:190–198, jan 2018.
- 561 [49] Ariel Ramírez-Torres, Salvatore Di Stefano, Alfio Grillo, Reinaldo Rodríguez-Ramos, José Merodio,  
562 and Raimondo Penta. An asymptotic homogenization approach to the microstructural evolution of  
563 heterogeneous media. *International Journal of Non-Linear Mechanics*, jul 2018.
- 564 [50] Kay Raum, Robin O Cleveland, Françoise Peyrin, and Pascal Laugier. Derivation of elastic stiffness  
565 from site-matched mineral density and acoustic impedance maps. *Physics in Medicine and Biology*,  
566 51(3):747–758, jan 2006.
- 567 [51] A. Reuss. Berechnung der Fließgrenze von Mischkristallen auf Grund der Plastizitätsbedingung für  
568 Einkristalle . *ZAMM - Zeitschrift für Angewandte Mathematik und Mechanik*, 9(1):49–58, 1929.
- 569 [52] Reinaldo Rodríguez-Ramos, Federico J. Sabina, Raúl Guinovart-Díaz, and Julián Bravo-Castillero.  
570 Closed-form expressions for the effective coefficients of a fiber-reinforced composite with transversely  
571 isotropic constituents – i. elastic and square symmetry. *Mechanics of Materials*, 33(4):223–235, apr  
572 2001.
- 573 [53] E. Rohan, S. Naili, R. Cimirman, and T. Lemaire. Multiscale modeling of a fluid saturated medium  
574 with double porosity: Relevance to the compact bone. *Journal of the Mechanics and Physics of Solids*,  
575 60(5):857–881, may 2012.
- 576 [54] Federico J. Sabina, Reinaldo Rodríguez-Ramos, Julián Bravo-Castillero, and Raúl Guinovart-Díaz.  
577 Closed-form expressions for the effective coefficients of a fibre-reinforced composite with transversely  
578 isotropic constituents. II: Piezoelectric and hexagonal symmetry. *Journal of the Mechanics and Physics  
579 of Solids*, 49(7):1463–1479, jul 2001.
- 580 [55] Enrique Sanchez-Palencia. *Non-Homogeneous Media and Vibration Theory*. Springer Berlin Heidelberg,  
581 1980.

- 582 [56] J.A. Sanz-Herrera, J.M. García-Aznar, and M. Doblaré. Micro-macro numerical modelling of bone  
583 regeneration in tissue engineering. *Computer Methods in Applied Mechanics and Engineering*, 197(33-  
584 40):3092–3107, jun 2008.
- 585 [57] I. S. Sokolnikoff. *Mathematical theory of elasticity*. McGraw–Hill, New York, 1956.
- 586 [58] J. J. Telega, A. Galka, and S. Tokarzewski. Application of the reiterated homogenization to determina-  
587 tion of effective noduli of a compact bone. *Journal of Theoretical and Applied Mechanics*, 37:687–706,  
588 1999.
- 589 [59] Sara Tiburtius, Susanne Schrof, Ferenc Molnár, Peter Varga, Françoise Peyrin, Quentin Grimal, Kay  
590 Raum, and Alf Gerisch. On the elastic properties of mineralized turkey leg tendon tissue: multiscale  
591 model and experiment. *Biomechanics and Modeling in Mechanobiology*, 13(5):1003–1023, jan 2014.
- 592 [60] D. Trucu, M.A.J. Chaplain, and A. Marciniak-Czochra. Three-scale convergence for processes in het-  
593 erogeneous media. *Applicable Analysis*, 91(7):1351–1373, jul 2012.
- 594 [61] Dimitrios Tsalis, Nicolas Charalambakis, Kevin Bonnay, and George Chatzigeorgiou. Effective proper-  
595 ties of multiphase composites made of elastic materials with hierarchical structure. *Mathematics and*  
596 *Mechanics of Solids*, 22(4):751–770, dec 2015.
- 597 [62] S. Weiner and H. D. Wagner. THE MATERIAL BONE: Structure-mechanical function relations. *Annual*  
598 *Review of Materials Science*, 28(1):271–298, aug 1998.
- 599 [63] Dan Wu, Per Isaksson, Stephen J. Ferguson, and Cecilia Persson. Young’s modulus of trabecular bone  
600 at the tissue level: A review. *Acta Biomaterialia*, aug 2018.
- 601 [64] Wen Yang, Irene H. Chen, Bernd Gludovatz, Elizabeth A. Zimmermann, Robert O. Ritchie, and Marc A.  
602 Meyers. Natural flexible dermal armor. *Advanced Materials*, 25(1):31–48, nov 2012.
- 603 [65] Tarek I. Zohdi, J.Tinsley Oden, and Gregory J. Rodin. Hierarchical modeling of heterogeneous bodies.  
604 *Computer Methods in Applied Mechanics and Engineering*, 138(1-4):273–298, dec 1996.